AGU PUBLICATIONS

JGR

Journal of Geophysical Research: Earth Surface

RESEARCH ARTICLE
10.1002/2014JF003232

Key Points:
- Hillslope erosion and runoff are simulated with a hydrogeomorphic model
- A stochastic approach is used to assess change in runoff and sediment yield
- Stochastic variability makes more uncertain sediment yield than runoff changes

Supporting Information:
- Readme
- Table S1
- Table S2

Correspondence to:
A. Francipane,
antonio.francipane@unipa.it

Citation:
Francipane, A., S. Fatichi, V. Y. Ivanov, and L. V. Noto (2015), Stochastic assessment of climate impacts on hydrology and geomorphology of semiarid headwater basins using a physically based model, *J. Geophys. Res. Earth Surf.*, *120*, 507–533, doi:10.1002/2014JF003232.

Received 4 JUN 2014
Accepted 3 FEB 2015
Accepted article online 6 FEB 2015
Published online 14 MAR 2015

Stochastic assessment of climate impacts on hydrology and geomorphology of semiarid headwater basins using a physically based model

A. Francipane[1], S. Fatichi[2], V. Y. Ivanov[2,3], and L. V. Noto[1]

[1]Dipartimento di Ingegneria Civile, Ambientale, Aerospaziale, dei Materiali, Università degli Studi di Palermo, Palermo, Italy, [2]Institute of Environmental Engineering, ETH Zürich, Zürich, Switzerland, [3]Department of Civil and Environmental Engineering, University of Michigan, Ann Arbor, Michigan, USA

Abstract Hydrologic and geomorphic responses of watersheds to changes in climate are difficult to assess due to projection uncertainties and nonlinearity of the processes that are involved. Yet such assessments are increasingly needed and call for mechanistic approaches within a probabilistic framework. This study employs an integrated hydrology-geomorphology model, the Triangulated Irregular Network-based Real-time Integrated Basin Simulator (tRIBS)-Erosion, to analyze runoff and erosion sensitivity of seven semiarid headwater basins to projected climate conditions. The Advanced Weather Generator is used to produce two climate ensembles representative of the historic and future climate conditions for the Walnut Gulch Experimental Watershed located in the southwest U.S. The former ensemble incorporates the stochastic variability of the observed climate, while the latter includes the stochastic variability and the uncertainty of multimodel climate change projections. The ensembles are used as forcing for tRIBS-Erosion that simulates runoff and sediment basin responses leading to probabilistic inferences of future changes. The results show that annual precipitation for the area is generally expected to decrease in the future, with lower hourly intensities and similar daily rates. The smaller hourly rainfall generally results in lower mean annual runoff. However, a non-negligible probability of runoff increase in the future is identified, resulting from stochastic combinations of years with low and high runoff. On average, the magnitudes of mean and extreme events of sediment yield are expected to decrease with a very high probability. Importantly, the projected variability of annual sediment transport for the future conditions is comparable to that for the historic conditions, despite the fact that the former account for a much wider range of possible climate "alternatives." This result demonstrates that the historic natural climate variability of sediment yield is already so high, that it is comparable to the variability for a projected and highly uncertain future. Additionally, changes in the scaling relationship between specific sediment yield/runoff and drainage basin area are detected.

1. Introduction

Soil erosion due to rainfall detachment and flow entrainment of soil particles are physical processes governing the continuous evolution of landscapes in many regions of the world. Most of their controlling factors, such as climate, hydrologic regime, geomorphic characteristics, soil type, and vegetation cover, are interrelated at the hillslope-watershed scales and determine soil erosion magnitude and its variations in space and time [*Istanbulluoglu,* 2009a, 2009b; *Nunes and Nearing*, 2010]. Among these controls, climate is an external factor that plays the key role in the dynamics of the erosion process. Given the overall complexity of the processes that are involved, the relationship between basin erosion rates and climate is not straightforward to capture [*Favis-Mortlock and Boardman*, 1995; *Imeson and Lavee*, 1998; *Pruski and Nearing,* 2002a, 2002b; *Nunes and Nearing*, 2010; *Mullan*, 2013]. While soil erosion rates are expected to change in response to climate perturbations, these changes can be highly nonlinear and catchment specific, making any generalization difficult [*Coulthard et al.,* 2012; *Nunes et al.,* 2013].

A significant body of research has been carried out on impacts of climate on landscapes and many studies have clearly shown the strong influence of climate on basin sediment yields [*Langbein and Schumm*, 1958; *Walling and Kleo*, 1979; *Roering et al.,* 2001; *Zhang et al.,* 2001; *Nunes and Nearing*, 2010; *Chen et al.,* 2011; *Naik and Jay*, 2011; *Phan et al.,* 2011; *Coulthard et al.,* 2012; *Nunes et al.,* 2013; *Shrestha et al.,* 2013] and landscape morphology [*Hack and Goodlett*, 1960; *Osterkamp et al.,* 1995; *De Boer and Crosby*, 1996; *Goodrich et al.,* 1997;

Dedkov, 2004; *Birkinshaw and Bathurst*, 2006; *Lane*, 2013]. Given the general paucity of sediment transport and erosion observations and the importance of analyzing projections for the future, numerical modeling is an appropriate approach for investigating complex climate-hydrology-geomorphology interactions [*Martin and Church*, 2004; *Nunes and Nearing*, 2010; *Martin*, 2013]. By incorporating the capability to describe multiple physical processes that are difficult to quantify in an experimental setting, numerical models, when successfully calibrated and confirmed, can alleviate problems associated with small-scale experiments or sparse observations. A number of modeling studies have been developed to explore the impacts of climate change on basin sediment response for a range of time and space scales, and examples of the approaches and limitations are presented by *Coulthard et al.* [2012], *Mullan et al.* [2012], and *Nunes et al.* [2013]. Early studies typically focused on hillslope erosion [*Favis-Mortlock and Savabi*, 1996; *Favis-Mortlock and Guerra*, 1999; *Nearing*, 2001; *Pruski and Nearing*, 2002a; *Nearing et al.,* 2005] and clearly demonstrated that soil erosion can respond both to changes in the total amount of rainfall and rainfall intensity [*Pruski and Nearing*, 2002a; *Römkens et al.,* 2002; *Nearing et al.,* 2005; *Nunes and Nearing*, 2010]. Such studies have been primarily based on the Water Erosion Prediction Project (WEPP) soil erosion model [*Nearing et al.,* 1989; *Laflen et al.,* 1991]. For example, *Favis-Mortlock and Guerra* [1999] used Global Circulation Model (GCM) climate projections to investigate changes in erosion rates. *Pruski and Nearing* [2002a] forced the WEPP model with hypothetical fractional changes of annual rainfall for a combination of soils, slopes, and crop types for several locations. Similarly, *Pruski and Nearing* [2002b] and *O'Neal et al.* [2005] applied the WEPP model to investigate potential changes in soil erosion rates in the Midwestern U.S. using synthetic daily climatology generated with the stochastic weather generator CLImate GENeration (CLIGEN) [*Nicks and Gander*, 1994] and downscaled GCM projections. *Zhang* [2007] tested the impacts of different downscaling methods on WEPP predictions, pointing out the importance of appropriate GCM projection downscaling. Using long-term climate scenarios of daily climate series, *Kim et al.* [2009] applied CLIGEN and the WEPP model to investigate the sensitivity of erosion process to precipitation representation. *Mullan* [2013] applied the WEPP model to six case study hillslopes in Northern Ireland using a Statistical Downscaling Model [*Wilby and Dawson*, 2007], demonstrating a potential increase in soil erosion in future climate conditions.

Modeling applications using various catchment-scale models have led to inferences regarding larger-scale process interactions. For example, erosion has been shown to be more sensitive to changes in rainfall intensity rather than rainfall amount, especially in semiarid and arid regions [*Nearing et al.,* 2005; *Nunes and Nearing*, 2010], where sparse vegetation (mainly in the form of shrubs) does not effectively shield soil from the erosive action of rain [*Riebe et al.,* 2001]. *Chaplot* [2007] applied an erosion component of the Soil and Water Assessment Tool (SWAT) model [*Neitsch et al.,* 2002] to two watersheds with humid and semiarid climates using synthetic series that assumed an amplification of observed rainfall. *Nunes et al.* [2008] applied the SWAT model to two groups of watersheds in Portugal with humid and semiarid climates using CLIGEN to simulate the projected temperature increase and a rainfall decrease in the area, pointing to rainfall changes as the main driving force to alter soil erosion regime. *Nunes et al.* [2013] used climate projections to explore the impacts on basin saturation deficit and vegetation cover affecting erosion processes and sediment yield with the MEFIDIS (Modelo de Erosão Físico e DIStribuído – Spatially Distributed Physical Erosion Model) model [*Nunes et al.,* 2005], demonstrating that the process interplay can offset positive response to increasing rainfall rates and exhibit scale dependence. *Routschek et al.* [2014] used a comprehensive EROSION 3D model [*von Werner*, 1995] to quantify the impact of climate change on soil loss at a catchment scale at high temporal and spatial resolution. Climate forcing for the period of 2031–2050 was generated with the WETTREG (weather situation-based regression method – in German: WETTerlagen-basierte REGressionsmethode) [*Enke and Spekat*, 1997; *Enke et al.,* 2005], which is a statistical downscaling method able to generate precipitation with high resolution (including extreme rainfall events) from GCMs outputs. Simulations with EROSION 3D showed that the impact of expected increase of precipitation intensities leads to a significant increase of soil loss.

Some of the limitations of the above studies include coarse spatial resolutions, possibly because of the need to deal with computational challenges, thereby obscuring the significance of the controlling effect of topography [*Kim et al.,* 2013; *Kim and Ivanov*, 2014]. Importantly, most of the climate change impact studies treated rainfall process overly simplistically, typically using daily events with the exceptions of studies by *Routschek et al.* [2014] and by *Coulthard et al.* [2012] (see below). Since the process of erosion is strongly and nonlinearly affected by the higher percentiles of rainfall intensity and magnitude (i.e., extreme events), higher-resolution characterization of rainfall is warranted for climate impact assessment studies [e.g., *Mullan et al.*, 2012].

At the other end of the spectrum, landscape evolution models (LEMs) were designed to examine connections between geomorphic processes and resulting landforms. The main limitation of LEMs is that they represent climate over long time scales (millennial scales), often in terms of mean magnitudes of precipitation and temperature [e.g., *Tucker and Slingerland*, 1997; *Tucker and Bras*, 2000; *Tucker et al.*, 2001a; *Temme et al.*, 2009; *van Balen et al.*, 2010], thereby ignoring details of the coupled hydrogeomorphic response to extreme rainfall. Only few LEMs operating at intermediate time scales have been adapted to integrate a more sophisticated representation of hydrological processes [*Hancock et al.,* 2011]. For example, CAESAR [*Coulthard et al.,* 2002, 2005] introduced a topography-driven, quasi steady state description of the hydrological response. The model has been used for a variety of temporal scales, from millennial [*Coulthard and Macklin*, 2001; *Van De Wiel et al.,* 2007] and centennial [*Welsh et al.,* 2009], to storm event scales [*Hancock and Coulthard*, 2012].

As mentioned, one notable exception to the major body of research on climate change impacts on hydrogeomorphic processes is a study by *Coulthard et al.* [2012]. Specifically, this study for the first time explicitly recognized that errors in climate change projections (with a resultant "cascade" propagation) and the short observational records representing historical dynamics cause large uncertainties in characterizing both high- and low-order moment properties of erosion and sediment transport characteristics. *Coulthard et al.* [2012] therefore chose a stochastic approach for representing both the historic conditions and the future, which allowed an evaluation of the effects of climate change on watershed geomorphic response in probabilistic terms. Hourly "baseline" (historic) and multiple climate projection rainfall scenarios were generated with a weather generator [*Murphy et al.,* 2009] to drive the CAESAR model. When applied to a midsize catchment in UK, their results demonstrated that a large fraction of projection uncertainty can be related to natural variability, also demonstrating a possible amplification of extreme runoff and erosion responses to climate change.

Another compounding problem in generalization of climate change impacts is that the basin geomorphic regime may exhibit scaling properties with catchment dimension. Several field studies suggested that sediment yield per unit area and sediment delivery ratio decrease as the basin area grows, following a power law with an exponent ranging between −1 and 0 [*Walling*, 1983; *Morris and Fan*, 1998; *Lu et al.,* 2005; *Parsons et al.,* 2006; *de Vente et al.,* 2007]. This inverse relationship can be explained by a decrease in slope and channel gradients, and hence in energy for sediment transport, as the basin size increases [*Birkinshaw and Bathurst*, 2006]. Similarly, as the distance between hillslope sediment sources and channels grows, so does the chance of deposition occurrence in wide valley floors and channels bars [*Birkinshaw and Bathurst*, 2006]. Still, a number of recent studies have indicated that the relationship between sediment yield and basin scale is complex because, unlike transport capacity, supply conditions may not change in a straightforward manner with basin scale [e.g., *De Boer and Crosby*, 1996; *Dedkov*, 2004].

Similar to the approach of *Coulthard et al.* [2012], this research stems from the understanding that any characterization of change of hydrogeomorphic states and fluxes should account for the variability of both the historic conditions as well as uncertainties associated with projections of the future. The study focuses on the U.S. Southwest, which is projected to become drier in the decades to come, with an overall increase of temperature and an increase of mean annual precipitation with less frequent rainfall events but of higher intensity [*Easterling et al.,* 2000; *Christensen et al.,* 2007; *Seager*, 2007; *Seager et al.,* 2007]. While the region is expected to become drier on average, the warmer atmosphere can create conditions that potentially could lead to larger and more frequent floods by causing more intense, heavy rainfall events [*Fowler and Hennessy*, 1995; *Intergovernmental Panel on Climate Change*, 2007; *Kunkel et al.,* 2010; *Wang et al.,* 2010]. The specific objective of this study is to investigate the effect of projected future climate conditions on mean and extreme runoff and sediment yield for semiarid watersheds of zeroth to first order, accounting for the uncertainty related to climate change predictions as well as stochastic climate variability. The spatially distributed, process-based hydrological model tRIBS, the Triangulated Irregular Network (TIN)-based Real-time Integrated Basin Simulator [*Ivanov et al.*, 2004a, 2004b], is used in combination with its integrated geomorphic component, tRIBS-Erosion [*Francipane*, 2010; *Francipane et al.,* 2012]. Climate forcing scenarios for historical and future conditions are generated using the Advanced Weather Generator (AWE-GEN) and a stochastic downscaling methodology [*Fatichi et al.,* 2011, 2013]. Climate scenarios are used as input to the model that is applied to a set of nested headwater basins in the Walnut Gulch Experimental Watershed (WGEW) [*Goodrich et al.,* 2008b; *Nearing et al.,* 2008] to yield probabilistic descriptions of basin responses to climate change in

terms of runoff and sediment yield. Moreover, since the approach is applied to basins different in size but similar in morphology, climate, and vegetation, the influence of climate change on scaling relationships of runoff and specific sediment yield with drainage area is also investigated.

2. Study Catchments

Climate, hydrology, digital elevation model (DEM), and land use data were combined for seven headwater basins nested within the Walnut Gulch Experimental Watershed (WGEW) in southeastern Arizona, USA (31.7166°N, 110.6833°W) [*Renard et al.,* 1993; *Ritchie et al.,* 2005; *Goodrich et al.,* 2008b; *Nearing et al.,* 2008; *Francipane et al.,* 2012]. These watersheds are identified by a three-digit code (i.e., Basin 102, Basin 104, Basin 105, Basin 106, Basin 121, and Basin 125), with the exception for Basin 101-103, which is composed of Basins 101 and 103. Their areas range between 0.26 and 6.7 ha and elevation ranges between 1334 and 1388 m above sea level (asl; Figure 1). Basins 101-103, 102, 104, 105, and 106 are adjacent (Figure 1), while Basins 121 and 125 are located about 2 km farther south. Most of the catchments exhibit morphology with steeper slopes in the middle of the flow path. Slopes range between 0% and 44.29% (24°). Climate, vegetation, and soil type are very similar and assumed to be identical for all basins.

Average annual precipitation for the period 1956–2005, calculated as the average of total rainfall at six rain gauges distributed over the entire basin [*Goodrich et al.,* 2008a, 2008b], is approximately 312 mm, 60% of which falls during the summer monsoon between July and September [*Goodrich et al.,* 2008a, 2008b]. Runoff regime is typical of many semiarid regions, where channels are dry for most time of the year. Typically, streamflow occurs as a result of intense thunderstorm rainfall, flood peaks arrive very quickly after the start of runoff generation, and runoff duration is short (e.g., from 40 min for the smaller watersheds to over 300 min for the large watersheds [*Stone et al.,* 2008]). Runoff is produced by the infiltration-excess mechanism [*Francipane et al.,* 2012]. The mean annual temperature is 18°C, with average monthly maximum temperatures of 35°C in June and average monthly minimum temperatures of 2°C in December. Vegetation in the area is dominated by desert shrub and semiarid rangeland plants. The dominant vegetation types are creosote bush (*Larrea tridentada*, shrub) with 2–5 m spacing and whitethorn (*Acacia constricta*, shrub). Desert zinnia (*Zinnia acerosa*, shrub), tarbush (*Flourensia cernua*, shrub), and black grama (*Bouteloua eriopoda*, grass) are present but less frequent. Larger creosote shrubs are about 1 m tall and can be characterized by spatially averaged leaf area index of 0.4 [*Flerchinger et al.,* 1998; *Fatichi et al.,* 2012]. Canopy cover during the rainy season is approximately 25–35% [*Weltz et al.,* 1994; *King et al.,* 2008; *Skirvin et al.,* 2008]. The dominant soil type is the McNeal gravelly sandy loam (60% sand, 25% silt, and 15% clay) with approximately 25% of rock fragments in the surface layer [*Francipane*, 2010]. The range in rock fragments ($>$2 mm) for the 0–25 cm soil layer is between 18% and 59% [*Ritchie et al.,* 2005]. Table 1 reports a summary of the principal characteristics of the catchments. For each basin, a DEM with a grid resolution of 10 m $\times$ 10 m has been downloaded from the official WGEW website. All of the data used in this study are available at http://www.tucson.ars.ag.gov/dap/.

3. Models, Data, and Methods

3.1. tRIBS: Hydrological Model

The TIN (Triangulated Irregular Network)-based Real-time Integrated Basin Simulator, tRIBS [*Ivanov et al.*, 2004a, 2004b], is a hydrological model that reproduces essential hydrologic processes in a river basin. The watershed topography is represented using a multiple-resolution approach based on TIN. The model uses a Voronoi polygon network (VPN), which offers a flexible computational structure reducing the number of computational elements without a significant loss of information [*Vivoni et al.,* 2004]. This permits the simulation of basin hydrological processes at very fine temporal (minutes to hour) and spatial (10–100 m) resolutions, stressing the role of topography in lateral soil moisture redistribution, by accounting for the effects of heterogeneous and anisotropic soil. A brief outline of the implemented process parameterizations is provided in the following:

1. Precipitation interception is simulated with the Rutter canopy water balance model [*Rutter et al.,* 1972, 1975] at the hourly time step. Canopy characteristics can vary for different vegetation types and are assigned based on values published in literature.
2. Surface energy budget is simulated at each computational element at the hourly scale accounting for shortwave and longwave radiation components that depend on geographic location, time of year,

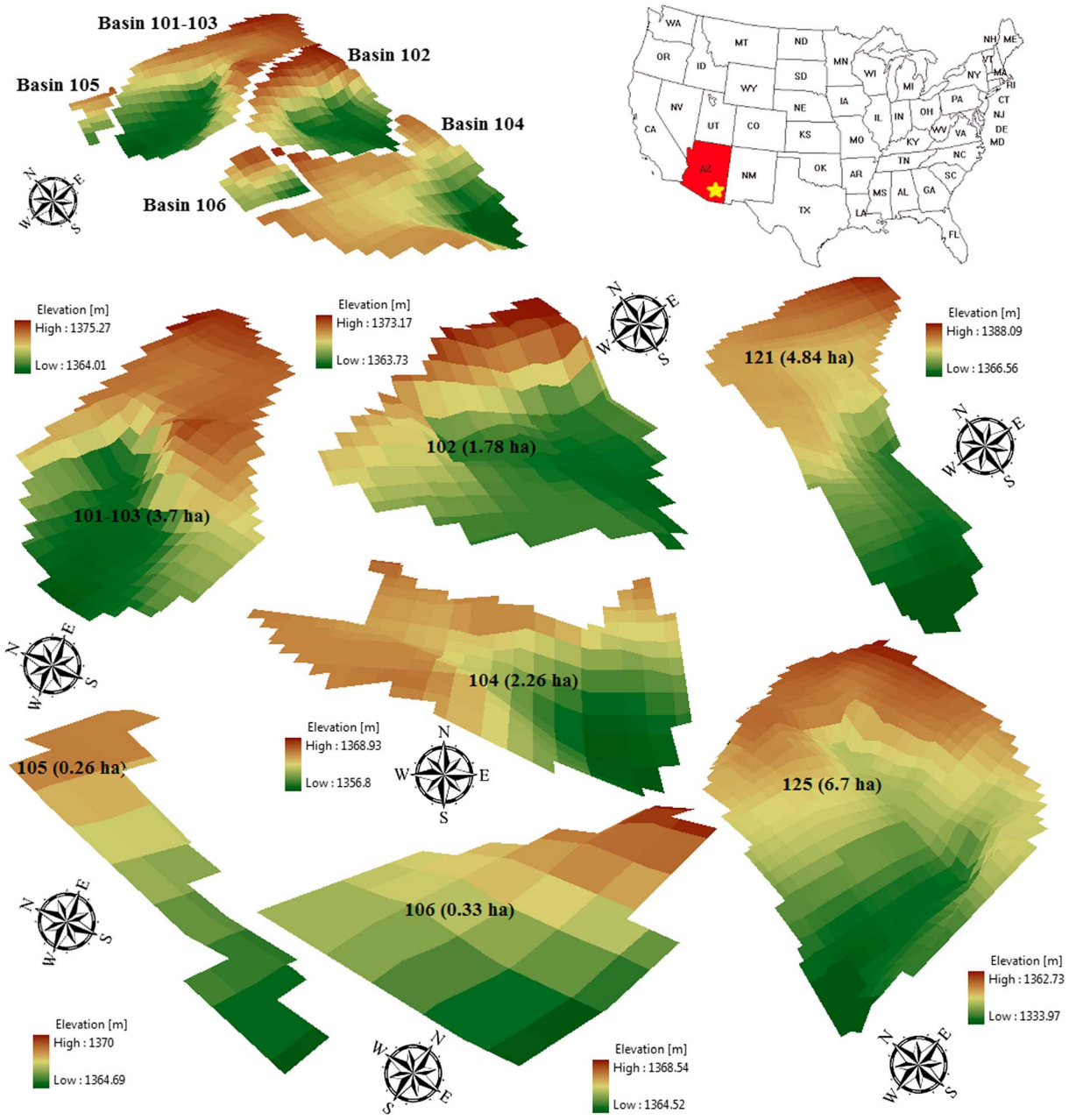

Figure 1. Digital elevation models (DEMs) of study basins. Grid resolution equals to 10 × 10 m. Headwater areas of Basins 101-103, 102, 104, 105, and 106 are adjacent. Basins 121 and 125 are located about 2 km farther south.

aspect, and slope of the element surface. The Penman-Monteith evapotranspiration model [*Penman*, 1948; *Monteith*, 1965], the gradient method [*Entekhabi*, 2000], and the force-restore ground heat flux approach [*Lin*, 1980; *Hu and Islam*, 1995] are used to estimate the latent, sensible, and ground heat fluxes at the land surface.

3. For simulating the process of infiltration, an assumption of gravity-dominated flow in a sloped column of heterogeneous, anisotropic soil is used, so that the effect of capillary forces is approximated [*Ivanov et al.*, 2004b]. The model of infiltration process simulates the evolution of wetting fronts that may lead to unsaturated, perched groundwater and completely saturated states. The first two cases represent states when the soil infiltration capacity is not constrained by the conductivity at the surface. The surface-saturated state is generated when the soil's infiltration capacity is constrained by the entire saturated profile.

Table 1. Essential Characteristics of Study Basins

Characteristics	Basin 101-103	Basin 102	Basin 104	Basin 105	Basin 106	Basin 121	Basin 125
Area (km^2)	0.037	0.0178	0.0226	0.0026	0.0033	0.0484	0.067
Elevation range (m)	11.26	9.44	12.13	5.31	4.02	21.53	28.76
Mean elevation (m)	1370.39	1367.85	1363.10	1363.34	1366.54	1379.64	1352.82
Minimum slope (%)	0.15	0.10	0.00	1.05	0.77	0.02	0.13
Maximum slope (%)	33.80	26.16	15.94	6.45	7.19	21.53	44.29
Mean slope (%)	6.29	7.52	6.03	3.44	3.98	5.47	9.70
Annual rainfall (mm)				312			
Land use/plant community				Shrub-dominated rangeland			
Plant cover (%)				25%			
Soil type				Gravelly sandy loam			

4. The groundwater dynamics are modeled based on the Boussinesq equation under the Dupuit-Forchheimer assumptions for lateral flows in the saturated zone [e.g., *Freeze and Cherry*, 1979, p. 180], allowing for lateral water redistribution in the saturated zone and its dynamic interactions with the unsaturated zone.
5. Runoff generation is made possible via four mechanisms: saturation excess, infiltration excess, perched subsurface stormflow, and groundwater exfiltration. Runoff is generated by representing the movement of infiltration fronts, water table fluctuations, and lateral moisture fluxes in the unsaturated and saturated zones. The computed runoff is used as input to the hydrologic (hillslope) and hydraulic (channel) flow models. Runoff flows along the edges of the watershed TIN in accordance with predetermined drainage directions (gradient of topographic surface).
6. A snowpack dynamic model [*Rinehart et al.,* 2008] permits the simulation of energy and mass budgets of snow-covered areas.

A full detailed description of the processes modeled in tRIBS is given in *Ivanov et al.* [2004b], while a discussion of the model performance is provided in *Ivanov et al.* [2004a].

3.2. tRIBS-Erosion: Geomorphic Component

The geomorphic component of tRIBS [*Francipane et al.,* 2012] formulates sediment flux equations for the processes of rainfall detachment and sheet erosion entrainment, combined with the continuity of mass to compute sediment dynamics across the landscape. The rate of change in landscape elevation, $\partial z/\partial t$, is assumed to be equal to a smaller value of local detachment/entrainment capacity and divergence of sediment flux (i.e., the excess sediment transport capacity [*Tucker and Slingerland*, 1997; *Tucker et al.*, 2001b]):

$$\frac{\partial z}{\partial t} = -\mathrm{Min}[D_c, \nabla q_s], \tag{1}$$

where Min is the minimum operator, D_c [L/T] is the detachment/entrainment capacity, q_s [L^3/LT] is the sediment load of overland flow, and ∇ is the divergence operator, i.e., the sediment transport capacity less the sum of incoming sediment fluxes, q_t, at a given location. The term D_c combines the capacities for sediment detached due to raindrop impact (rain splash) and sediment entrained in sheet overland flow. The rate of soil detachment due to raindrop impact energy, D_R [M/L^2T], is modeled with a conceptual approach of *Wicks and Bathurst* [1996], in which rain action is split between the effects of direct raindrop impact and that of leaf drip:

$$D_R = k_r F_w [C_R M_R + C_D M_D], \tag{2}$$

where k_r [$1/J$] is the raindrop soil erodibility and F_w is the shield effect of surface water. The variables M_R [M^2/T^3] and M_D [M^2/T^3] are the rainfall drop impact squared momentum and the leaf drip squared momentum, respectively [*Salles et al.,* 2000; *Styczen and Høgh-Schmidt*, 1988], used to represent splash of soil particles into the air. The variables C_R and C_D are weighted areal fractions that quantify the direct raindrop and leaf drip impacts on rain splash detachment. The fraction C_R is modeled as

$$C_R = \left(1 - C_p\right)\left[(1 - V) + pV\right], \tag{3}$$

where C_p is the fraction of Voronoi cell protected against drop erosion, V is the vegetation fraction of a Voronoi cell, and p is the throughfall coefficient for vegetation fraction, i.e., the fraction of rainfall over canopy not intercepted by vegetation. In equation (3), the terms $(1 - C_p)\,(1 - V)$ and $(1 - C_p)\,pV$ respectively represent splash erosion in bare soil and vegetated soil fractions of the Voronoi cell. The fraction C_D is modeled as

$$C_D = F_I\left(1 - C_p\right)\,(1\ - p)V, \tag{4}$$

where F_I [0 − 1] is the fraction of rainfall intercepted by canopy that reaches soil in the form of leaf drip.

The entrainment and transport of sediment by overland flow are estimated using shear stress-based formulations [*Yang*, 1996; *Nearing et al.,* 1999], without differentiating between overland and channel flows as the form of shear stress-based equations for both cases is nearly identical [*Francipane et al.,* 2012]. The effective boundary shear stress, τ [M/LT^2], is calculated according to a well-known power law function of local discharge and slope:

$$\tau = k_t q^{m_b} S^{n_b}, \tag{5}$$

where q [L^3/LT] is the local discharge per unit width of Voronoi edge, S [0–1] is the local slope, and m_b and n_b are empirical parameters [*Willgoose et al.,* 1991; *Istanbulluoglu et al.,* 2004]. Assuming locally uniform overland flow conditions and using Manning's equation for the flow velocity, m_b and n_b are equal to 0.6 and 0.7, respectively [*Tucker et al.,* 2001a]. The variable k_t [M/L^2T^2] depends on the Manning coefficient n as follows [*Simons and Şentürk*, 1992; *Tucker et al.,* 2001b; *Istanbulluoglu and Bras*, 2005]:

$$k_t = \frac{\rho_w g n_s^{1.5}}{\left(n_s + n_v\right)^{0.9}}, \tag{6}$$

where ρ_w is the water density [M/L^3], g is the acceleration due to gravity [L/T^2], n_s is the Manning roughness coefficient for soil, and n_v is the latter coefficient for vegetation.

The flow entrainment capacity, D_D [L/T], is calculated as

$$D_D = k_b(\tau - \tau_c)^{p_b}, \tag{7}$$

where k_b is the soil erosion efficiency coefficient [$L/T\ (M/LT^2)^{\ p_b}$], τ_c [M/LT^2] is a threshold stress for particle entrainment (i.e., "the critical shear stress"), and p_b is an empirical parameter equal to 2.3 [*Nearing et al.,* 1999].

The transport capacity, D_T [L^3/T], is calculated as

$$D_T = Wk_f(\tau - \tau_c)^{p_f}, \tag{8}$$

where W [L] is the channel width, considered to be equal to the width of the edge of a Voronoi cell [*Tucker et al.,* 2001b], p_f is a parameter equal to 2.5, and k_f is a coefficient for a single sediment size fraction [*Yalin*, 1972; *Simons and Şentürk*, 1992]:

$$k_f = k_k \frac{\sqrt{g(s-1)d^3}}{\left[\rho_w g(s-1)d\right]^{p_f}}, \tag{9}$$

where s is the ratio of sediment density to water density (taken as 2.65) and d is the dominant grain size [L], taken as d_{50}, i.e., the diameter corresponding to the 50% value of the granulometric distribution curve, and k_k is a calibration coefficient. The values of k_k have been reported to be in the range of 4–40 in different studies [*Yalin*, 1972].

In the application of equation (1), sediment is routed on a cell-by-cell basis following the direction of steepest descent. The detached/entrained sediment of an upstream Voronoi element (or multiple elements) enters a downstream cell and is used for calculating the divergence of sediment flux. In a continuous application of the geomorphic model to a watershed domain that has a spatially variable structure of hydrological states, the sediment accumulates or moves downstream and elevations change as a consequence of this transport process. Calculation starts at a Voronoi cell with the highest elevation and proceeds downstream to the basin outlet cell:

1. For each computational element, the rate of soil detachment by raindrop D_R and the entrainment capacity rate D_D are calculated using equations (2) and (7).

2. The transport capacity rate D_T is calculated using equation (8).
3. For each cell, the potential rate of transport-limited erosion, $\nabla q_s = -\frac{\Delta z_{i,\ \mathrm{pot}}}{\Delta t}$, where z_i and $\Delta z_{i,\ \mathrm{pot}}$ are the elevation and the potential elevation change at node i, respectively, is calculated as a function of D_T.
4. For each cell, the maximum potential rate of detachment/entrainment-limited erosion, $D_c = -\frac{\Delta z_{i,\ \mathrm{ava}}}{\Delta t}$, where z_i and $\Delta z_{i,\ \mathrm{ava}}$ are the elevation and the available elevation change at node i, respectively, is calculated based on the sum of rates D_R and D_D (conventionally, $\Delta z_{i,\mathrm{ava}}$ is always less than 0).
5. Finally, the two rate products (i.e., rate multiplied by a time step of 1 h) are compared to define local deposition and erosion and properly define flux downstream of a given Voronoi cell:

   a. If $\Delta z_{i,\mathrm{pot}} > 0$, *deposition* occurs and $\Delta z = \Delta z_{i,\mathrm{pot}}$;
   b. If $\Delta z_{i,\mathrm{ava}} < \Delta z_{i,\mathrm{pot}} < 0$ (*erosion*), then $\Delta z_i = \Delta z_{i,\mathrm{pot}}$ and *transport-limited erosion* occurs;
   c. If $\Delta z_{i,\mathrm{pot}} < \Delta z_{i,\mathrm{ava}} < 0$ (*erosion*), then $\Delta z_i = \Delta z_{i,\mathrm{ava}}$ and *detachment/entrainment-limited erosion* occurs.
   d. In the case when $|\Delta z_{i,\mathrm{pot}}| > |\Delta z_{i,\mathrm{ava}}|$, the transport capacity rate of the flow is not at the maximum value (i.e., detachment or entrainment-limited), and upon calculation of the actual erosion/deposition in a cell, the outgoing sediment flux from the cell under consideration into a downstream cell is redefined as a function of $\Delta z_{i,\mathrm{ava}}$.

At the hourly scale, the model updates the elevation of each Voronoi element and recomputes slopes, azimuthal aspects, flow directions, and drainage areas of the entire VPN, as well as re-sorts nodes according to the topography-dictated flow graph order. The latter is determined based on local maximum surface slopes [*Ivanov et al.,* 2004b], and the erosion process thus leads to a continuously updated drainage pattern. Since the topography of the catchment is updated, the geomorphic processes of erosion and deposition have the capability to feedback the hydrologic dynamics.

A comprehensive description of the processes modeled in tRIBS-Erosion is provided in *Francipane et al.* [2012]. The latter study also offers the results of a long-term calibration of runoff and sediment yield for the Lucky Hills basin (a basin nested within the WGEW) that served to provide model parameterization (Tables S1 and S2 in the supporting information) for assessment developed here. The implicit assumption is that the accepted model parameterization, partly based on calibration and partly on literature-inferred values, is suitable for representing geomorphic dynamics characteristic of headwater basins in the semiarid environment of the Walnut Gulch Experimental Watershed. As later comparison of scaling relationships demonstrates (see a discussion of Figure 14 in section 4.6), the chosen model formulation provides a consistent baseline for all of the basins, including six for which no prior calibration has been carried out. This therefore permits model use in a study addressing the differential effect of change in the forcing conditions.

3.3. Climate Data

In order to force the hydrogeomorphic model, time series of various meteorological variables are required. Specifically, the model needs hourly precipitation, air temperature, vapor pressure, wind speed, atmospheric pressure, and shortwave radiation. All of the required meteorological time series were collected for a relatively short period (July 1996 through December 2009) at the meteorological station US-Whs (31.7438°N, 110.0522°W, elevation 1372 m asl) within the Lucky Hills watershed [*Emmerich and Verdugo*, 2008; *Fatichi et al.,* 2012]. The US-Whs station is a part of AmeriFlux, a regional FLUXNET network that coordinates regional and global analysis of observations from numerous flux tower sites (http://public.ornl.gov/ameriflux/index.html). The relatively short duration of observations is insufficient to provide baseline climate characteristics that are responsible for runoff and sediment transport regimes of a semiarid system such as WGEW, since these regimes are affected by considerable interannual variability [*Polyakov et al.,* 2010]. Due to this reason, a longer record of observations for a meteorological station at Tucson airport (32.1145°N, 110.9392°W, elevation 792 m asl) for a period of 1961–2000 is used in this study. Tucson exhibits desert, semiarid climate with hot summers and temperate winters. Precipitation has a strong seasonality with about 50% falling during the summer monsoon period from July to September [*Sheppard et al.,* 2002]. The mean annual temperature is 20.2°C and the mean annual precipitation is 304 mm. Climate characteristics of Tucson are similar to those of Lucky Hills: Tucson is slightly warmer (+3°C) and drier (precipitation is less by 50 mm), mainly due to its lower elevation. Nonetheless, the climate of Tucson can be considered to be representative of the conditions of southeast Arizona [*Sheppard et al.,* 2002]. Therefore, climate characterized by the observational record from Tucson airport is used as a baseline for the generation of time series representative of present and future climates, as described below.

3.3.1. Generation of Climate Forcing With AWE-GEN

The Advanced Weather Generator (AWE-GEN) is a stochastic simulator designed to produce hourly time series of weather variables for a given stationary climate. In situ, point-scale observations are required for its parameterization [*Fatichi*, 2010; *Fatichi et al.,* 2011]. The generator simulates several types of climate variables:

1. Precipitation is the primary driving variable simulated using the Neyman-Scott rectangular pulse model [*Cowpertwait*, 1991; *Cowpertwait et al.*, 1996, 2007; *Paschalis et al.*, 2014]. The precipitation process is characterized using various statistics for aggregation intervals of 1, 6, 24, and 72 h. Seasonal variations are introduced by using month-specific parameter values. Interannual dynamics are imposed by simulating annual precipitation through an autoregressive order-one model [*Fatichi*, 2010; *Fatichi et al.,* 2011].
2. Cloud cover is simulated during interstorm periods, during which the existence of the stationary "fair weather" region is assumed. A dynamic transition of the cloud process between the boundary of a storm and the fair weather period is assumed.
3. Air temperature, vapor pressure, and wind speed are simulated using similar functional forms as a combination of deterministic components that introduce dependencies among meteorological variables (e.g., between rainy hours and cloud cover, changes in air temperature and Sun position, solar radiation, and wind speed) and stochastic components.
4. Shortwave radiation is simulated with a two-band atmospheric radiation transfer model for clear-sky conditions [*Gueymard*, 2008], modified to account for cloud cover [*Stephens*, 1978; *Slingo,* 1989]. For a complete description of the AWE-GEN model structure and parameterization, the reader is referred to *Fatichi et al.* [2011] and to the AWE-GEN technical reference (http://www.umich.edu/~ivanov/HYDROWIT/Models.html).

3.3.2. Generation of Baseline Climate Ensemble

Forty years of observed climate can be generally assumed to be sufficient to fully characterize the first two moments, i.e., the mean and the variance, of most of the observed meteorological variables such as air temperature, vapor pressure, and wind speed [*Peixoto and Oort*, 1992]. With regard to precipitation, however, such an observational period can yield only a fairly accurate estimate of the first moment at various temporal scales. Statistical characterization of rare events, such as very wet or dry periods as well as extreme rainfall, remains limited because of natural climate (stochastic) variability [*Deser et al.,* 2012a, 2012b; *Fatichi et al.,* 2013; *Fischer et al.,* 2013; *Fatichi et al.,* 2014]. As a result, the characterization of hydrogeomorphic fluxes that are driven by infrequent, extreme precipitation events is an even grander challenge. In a semiarid environment, this statement is well confirmed by the rare occurrence of runoff and sedimentation events [*Coppus and Imeson*, 2002; *Polyakov et al.,* 2010]. Sediment yield series, either observed or simulated for a 40 year period, are therefore only representative of a particular climate realization. The observed series can be used to evaluate the annual mean of sediment yield, yet with fairly large error bounds. For example, if annual yield could be considered a random variate following the normal distribution with unknown variance (an obvious simplification to illustrate the statement), the 5th and 95th percentile bounds of the distribution describing the mean value estimated from a record of length $n = 11–16$ (i.e., the number of observational years for a set of selected basins) would be ±30% to ±137% of the estimated mean value. Reliable assessment of variance of the process with such short records is practically impossible.

Consequently, in order to explore the natural (stochastic) variability of the reference climate and its impact on the basin hydrogeomorphic response, we used AWE-GEN to generate an ensemble of fifty 30 year long, hourly time series of meteorological variables representing realizations of climate consistent with observations in Tucson over the control period of 1961–2000. This set of realizations is referred to as the ConTrol Scenario (CTS) "ensemble" or "set." AWE-GEN parameter values are reported in *Fatichi* [2010] and *Fatichi et al.* [2011].

3.3.3. Generation of Future Climate Ensemble

A stochastic downscaling methodology is used to generate an ensemble of hourly time series of meteorological variables that express a set of possible future climate conditions for the location of Tucson. The stochastic downscaling uses realizations from GCMs and the hourly weather generator AWE-GEN. Procedural steps and theoretical assumptions of the methodology for generating the time series expressing the "most probable" future and/or an ensemble distribution of possible future scenarios are described in detail in *Fatichi et al.* [2011, 2013]. Only a brief outline is provided below:

1. Information on projected climate change is derived from realizations of GCMs. This study used projections obtained from the data set compiled in the World Climate Research Programme (WCRP), Coupled Model Intercomparison Project, Phase 3 (CMIP3) for the emission scenario A1B (a midrange positive radiative forcing scenario [*Meehl et al.*, 2007]). The GCM-derived time series of precipitation and temperature are used for estimation of daily, monthly, and annual statistics. For the GCM surface temperature time series, the means are computed at the monthly resolution. For the precipitation process, the mean, the variance, the skewness, and the frequency of nonprecipitation for different aggregation intervals are estimated (four statistics, four aggregation intervals, and 12 months). Additionally, to account for low-frequency properties of the precipitation process, the coefficient of variance and skewness is estimated.
2. The probabilistic distributions of "factors of change," which are either additive (for air temperature) or ratios (for precipitation) [*Anandhi et al.,* 2011; *Fatichi et al.,* 2011], are computed. They are derived from GCM realizations using a specific technique, a Bayesian methodology [*Tebaldi et al.,* 2004; *Tebaldi et al.,* 2005; *Fatichi et al.,* 2013], that weights different members of the GCM ensemble and produces a probability distribution function for each factor of change. Since AWE-GEN is a point-scale weather generator, accordingly, factors of change from climate models are estimated for grid cells nearest to Tucson. This assumption is reasonable, when one considers that spatial variability of factors of change among neighboring cells of a given GCM is rather small and definitely smaller than differences among GCMs [*Fatichi et al.,* 2011].
3. A Monte Carlo technique is consequently used to sample the factors of change from their respective marginal probability distributions, assuming specific cross correlations among the factors of change [*Fatichi et al.,* 2013]. In this study, 100 sets of factors of change are drawn to sample the frequency distributions of projected future climate statistics. Such a large ensemble is used to address the uncertainties of GCM simulations and partially account for stochastic climate variability due to the proximity of some of the climate trajectories imposed by factors of change obtained with Monte Carlo sampling [*Fatichi et al.,* 2013].
4. The factors of change are applied to the climate statistics derived from historical observations to reevaluate the parameters of the weather generator. In this study, 100 parameter sets for AWE-GEN are obtained, each corresponding to a future climate "alternative."
5. The final result of the procedure is the generation of hourly time series using the reevaluated parameter sets. An ensemble of one hundred 30 year long, hourly time series of meteorological variables is simulated with AWE-GEN. Each of the 100 series can be considered representative of the 2081–2100 future climate conditions. This set of realizations is referred to as the FUTure (FUT) "ensemble" or "set."

The above methodology represents the state-of-the-art of stochastic downscaling approaches: it permits the simulation of short temporal scales (hourly) and higher-order statistics (extremes) and allows one to concurrently account for the internal (stochastic) climate variability and the spread among climate model predictions, which are typically indicated as the principal uncertainty sources [*Räisänen*, 2007; *Hawkins and Sutton*, 2011; *Fatichi et al.,* 2014].

4. Results

Using the ensemble series of the CTS (ConTrol Scenario) and the FUT (FUTure scenario) sets, the tRIBS-Erosion model is forced to reproduce hydrogeomorphic responses of seven study basins (described in section 2) in terms of runoff and sediment yield.

4.1. Variability of Climate Forcing

Since rainfall characteristics of the study area are the main factors driving runoff and sediment yield, an analysis of both the CTS and the FUT climate ensembles is first developed.

Mean annual precipitation (MAP) is computed for each 30 year long climate ensemble member of the CTS and FUT scenarios. The interannual variability of precipitation of each climate realization is characterized using the standard deviation (STD) of annual rainfall. In order to assess the differences between precipitation forcings of the CTS and FUT ensembles, the cumulative density functions (CDFs, i.e., the probability that a variable takes on a value less than or equal to a given value) of MAP and STD are computed using 50 (for the CTS ensemble) or 100 (for the FUT ensemble) realizations and plotted in Figure 2. The CTS ensemble is characterized by a much smaller MAP variability in the ensemble set, with a mean value of ~300 mm/yr (Figure 2a). The corresponding relative variability among different 30 year realizations is assessed by the

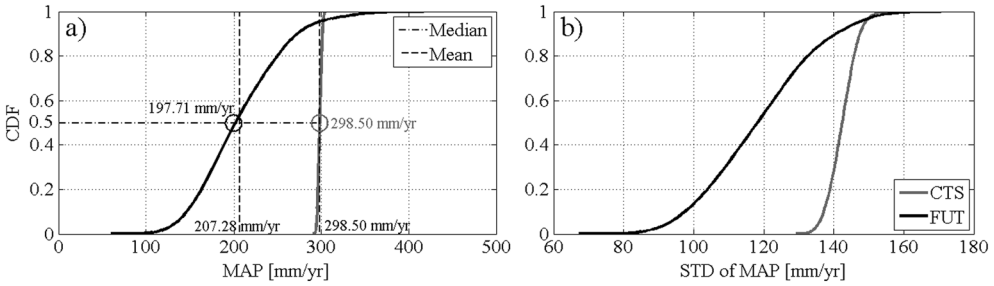

Figure 2. A statistical representation of precipitation forcing for the CTS (grey) and the FUT (black) ensembles simulated with the AWE-GEN model (a) the cumulative frequency distributions of 30 year mean annual precipitation (MAP) and (b) the cumulative frequency distributions of 30 year standard deviation (STD) are computed using the FUT and CTS ensembles. Magnitudes of the median and mean values of MAP are also shown in Figure 2a.

coefficient of variation, CV_E, which is equal to 0.65%. The FUT ensemble is characterized by a larger MAP variability ($CV_E = 21.83\%$), corresponding to a mean MAP value of ~207 mm/yr (Figure 2a). These differences are not surprising given the fact that the CTS set represents a single stationary climate, while the FUT ensemble is composed of 100 possible future climates determined from uncertain projections, which are not necessarily similar to each other.

Variations of interannual characteristics of precipitation among the members of the two ensembles are expressed through STD of annual precipitation, which is shown in Figure 2b in terms of CDFs of the 50 (the CTS set) and 100 (the FUT ensemble) STDs of annual precipitation. As seen in these plots, the annual precipitation of individual realizations of the FUT ensemble exhibits wider fluctuations, as compared to the annual precipitation of the CTS ensemble. This is a result of applying two factors of change in the downscaling methodology: one for coefficient of variation and the other for skewness of the annual precipitation [*Fatichi et al.,* 2011, 2013], as well as due to the overall uncertainty in representing the process at both short (event) and large (annual) scales.

Statistics of rainfall intensity obtained at the hourly scale (considering rainy hours only) are shown in Figures 3a and 3b where the curves of relative frequency of exceedance, i.e., the probability of rainfall being greater than or equal to a given value, of hourly and daily rainfall are shown. The FUT ensemble exhibits a larger variability of rainfall intensity, as compared to the CTS ensemble. This is another illustration of the high uncertainty characteristic of the projection of future climate conditions. Furthermore, the *median* relative frequencies of the exceedance curve of hourly rainfall for the CTS set are always higher than those of the FUT set (Figure 3a). Concurrently, the median relative frequencies of exceedance curves nearly overlap for the daily rainfall (Figure 3b). This leads to an inference that the projected future climate can be

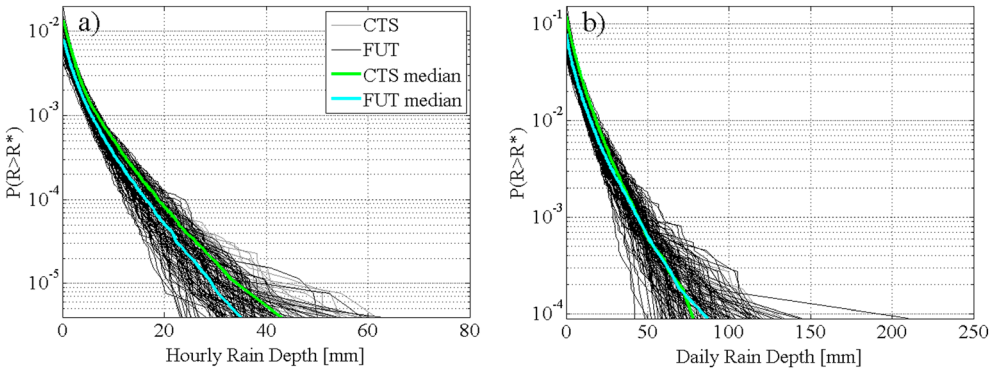

Figure 3. Curves of relative frequency of exceedance constructed for (a) hourly and (b) daily rainfall. The thin lines (grey or black) show the relative frequency of exceedance of individual ensemble members (CTS or FUT), while the thick lines (green or cyan) represent the median relative frequencies of exceedance of an ensemble (CTS or FUT).

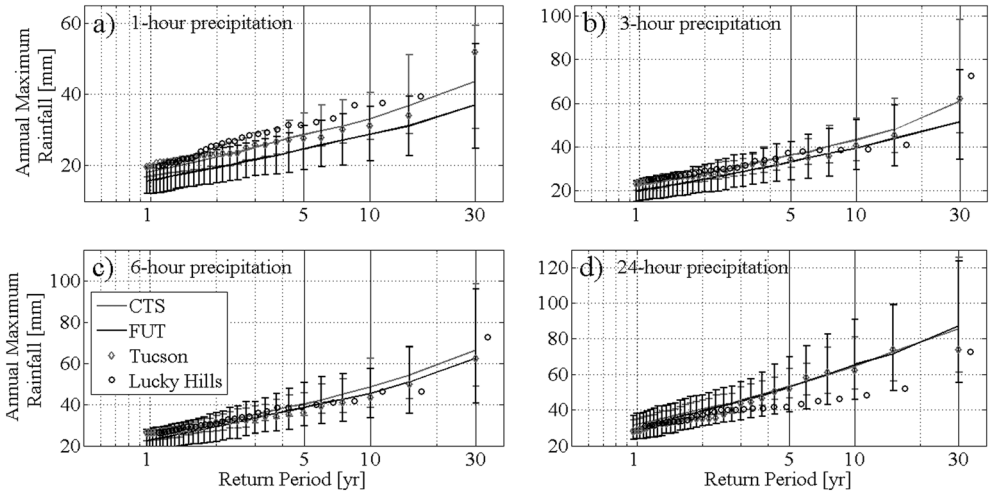

Figure 4. Changes in extreme rainfall events for (a) 1, (b) 3, (c) 6, and (d) 24 h durations. The confidence bounds correspond to the 5th and 95th percentile of the stochastic ensemble. Symbols for "Tucson" and "Lucky Hills" correspond to the observed data at these respective locations.

characterized by rainfall events with lower hourly intensities than the present climate, but with similar or larger (for the largest magnitudes) daily rainfall.

This aspect can be further explored by analyzing changes in extreme events for different durations. Annual maximum precipitation for different durations (1, 3, 6, and 24 h) is shown as a function of the return period in Figure 4. Future climate (black line) is generally characterized by extreme rainfall events with magnitudes lower than those in the present climate (grey lines) for shorter durations. However, the uncertainty of characterizing extremes is very high with a large overlap between the present and future climates, as testified by the 5th and 95th percentile bounds (the vertical bars). Moreover, one can also appreciate that the employed weather generator is capable of reproducing extreme precipitation events for different durations for the location of Tucson. Extreme events are also similar and within the confidence bounds for the location of Lucky Hills (Figure 4).

Besides precipitation forcing, AWE-GEN also generates synthetic time series of all other hydroclimatic variables necessary to force tRIBS-Erosion simulations. Figure 5 illustrates average daily cycles of most relevant variables used in hydrogeomorphic simulations. As seen, future climate is represented by higher daily air temperature (Figure 5a) and atmospheric longwave radiation (Figure 5c) and lower daily relative humidity (Figure 5b). This is consistent with the projected warmer and drier climate and therefore higher atmospheric moisture demand. Nearly the same daily incoming shortwave radiation (Figure 5d) cycle is obtained since the factor of change for this variable is not computed directly [*Fatichi et al.,* 2013]. However, shortwave radiation is not projected to significantly change in the future.

Overall, the differences between the CTS and FUT ensembles identified here, in terms of the mean annual and interannual variability of precipitation as well as event-scale precipitation statistics and other climate drivers, will be responsible for contrasting responses of basin runoff generation and sediment yield representing current and future conditions.

4.2. Runoff

For each of the catchments, tRIBS-Erosion is forced with ensemble members of the CTS and the FUT scenarios and the mean annual runoff normalized per unit area (MAR) is computed for each 30 year simulation. The interannual variability of runoff is characterized by estimating the standard deviation of annual runoff for each simulation. In order to assess the differences between the runoff characteristics of the CTS and FUT ensembles, the CDFs of MAR are computed using 50 (for the CTS ensemble) and 100 (for the FUT ensemble) simulations (Figure 6).

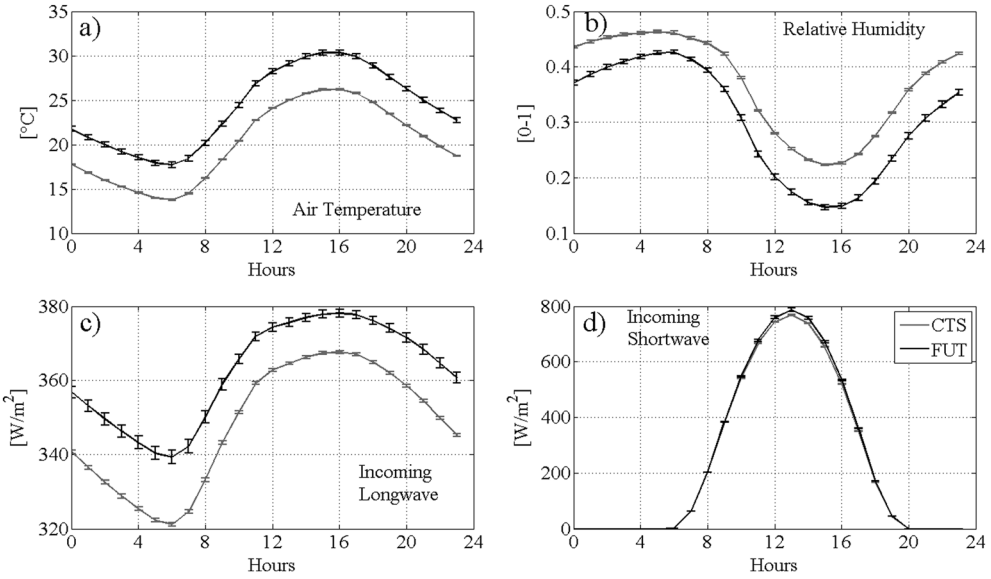

Figure 5. Mean diurnal cycles of several climate variables obtained by averaging over all realizations of the CTS (grey line) and the FUT (black line) ensembles simulated with AWE-GEN: (a) air temperature, (b) relative humidity, and incoming (c) longwave and (d) shortwave fluxes. The confidence bounds represent standard deviations estimated using the ensemble members (50 for CTS and 100 for FUT).

For all of the basins, MAR of the CTS ensemble is characterized by a lower variability, as compared to the FUT ensemble (Figure 6). The corresponding coefficient of variation, CV_E, is ~15% for all of the basins for the CTS, while this coefficient ranges between 46.6% (Basin 106) and 60.4% (Basin 125) for the FUT ensemble. These differences, which are expected, are a direct consequence of the variability underlying the CTS and FUT climate forcings. However, it is noteworthy that despite the fact that the mean annual rainfall of the CTS ensemble has a very low variability (Figure 2), the variability of runoff is much larger due

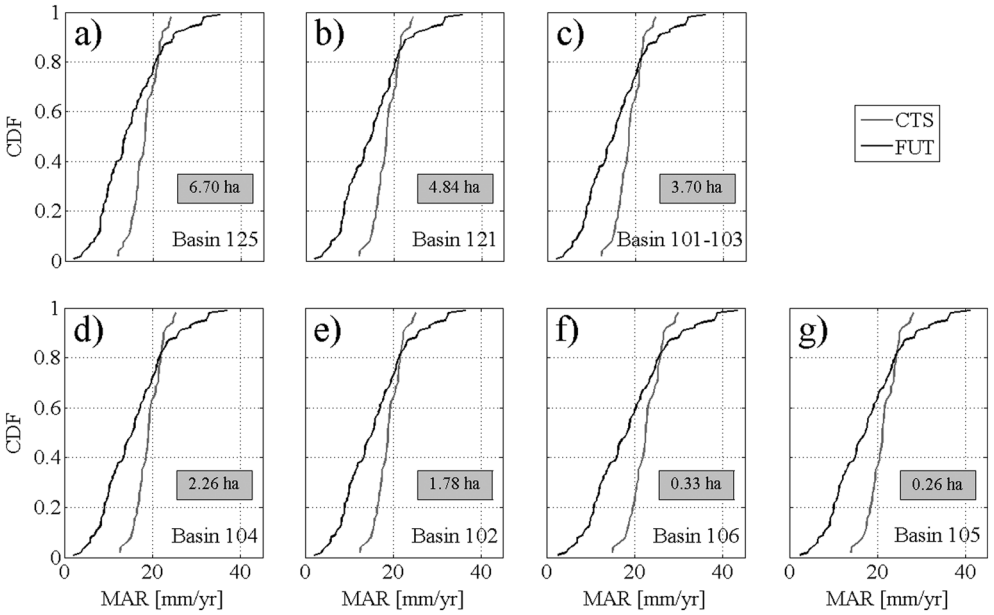

Figure 6. The cumulative frequency distributions of 30 year mean annual runoff (MAR) for the control (CTS, 50 realizations) and future (FUT, 100 realizations) climate ensembles. The results are presented for all seven basins arranged in the order corresponding to a decreasing area. The values in the grey boxes indicate respective basin areas in hectares.

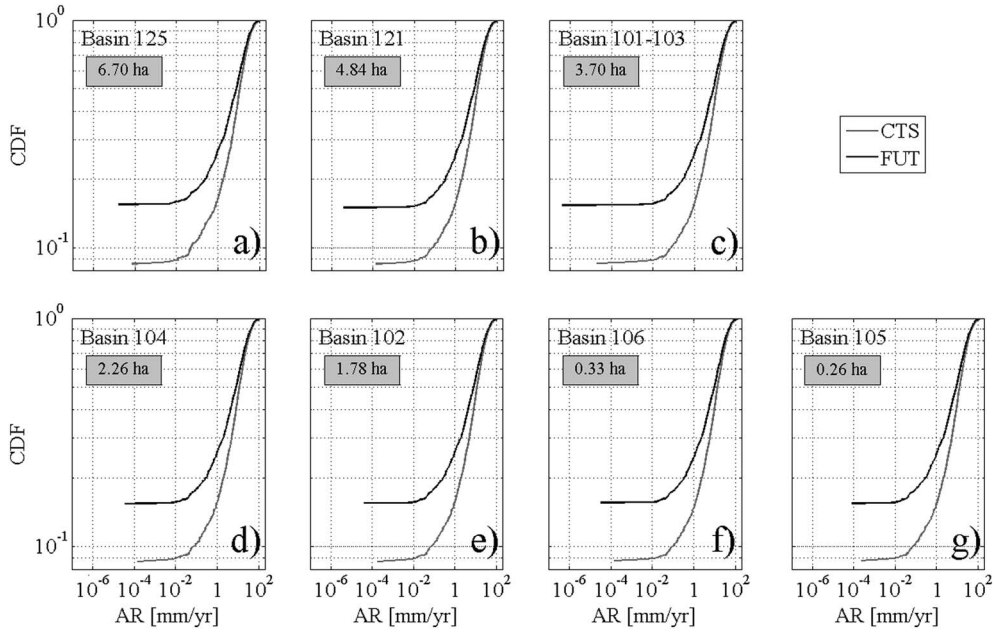

Figure 7. The cumulative frequency distributions of annual runoff, AR, for the control, CTS (50 scenarios, 30 year long each, or 1500 of simulated years in total), and future, FUT (100 scenarios, 30 year long each, or 3000 of simulated years in total), climate ensembles. The values in the grey boxes indicate respective basin areas in hectares.

to within year stochasticity. This can be also attributed to a threshold behavior in generation of runoff by the infiltration excess mechanism, which is predominant in this area and responsible for most of the simulated runoff (not shown). Overall, the mean streamflow in the future is projected to be lower than that in the present conditions (Figure 6): only 15–20% of the largest 30 year averaged runoff is expected to be higher for the FUT set (i.e., higher than the percentile value corresponding to the intersection of the black and grey lines).

When annual runoff (i.e., not averaged over 30 years of simulation) for both the CTS and the FUT ensembles is compared in terms of cumulative frequency distributions (Figure 7), one can infer that the distribution of projected future runoff is essentially to the left of the distribution corresponding to the present conditions. The differences in the probability of non-exceedance are remarkable especially during years with low runoff (Figure 7). One can consequently infer that the 15–20% possibility of increase of long-term runoff in the future inferred from Figure 6 is mainly explained by interannual variability, i.e., how different years are combined within an ensemble member. That is, a series of years with relatively large runoff represent a future alternative with higher runoff for the same MAR percentile value, as compared to the control conditions. This is in contrast to a hypothetical case of ensemble members exhibiting few years with runoff higher than in the CTS set, not obtained here (Figures 6 and 7).

4.3. Sediment Yield

The mean annual sediment yield normalized per unit area (MAS) for each 30 year long simulation is shown in Figure 8. The mean sediment yield increases with the basin area. On average, the long-term sediment yield is expected to decrease in the future with a very high probability: the black line (CDF of FUT) rarely crosses the grey line (CDF of CTS) in Figure 8. This occurs despite a non-negligible probability that mean runoff may in fact increase (Figure 6).

In contrast to the previous conclusion for runoff, the variability of sediment yield for the FUT ensemble is comparable to that for the CTS ensemble for all of the basins. The coefficient of variation CV_E of sediment yield exhibits a nearly robust negative dependence on the catchment area and ranges between 17.8% (Basin 101-103) and 93.7% (Basin 106) for the CTS set and between 38.3% (Basin 101-103) and 127% (Basin 106) for the FUT ensemble set (Figure 8).

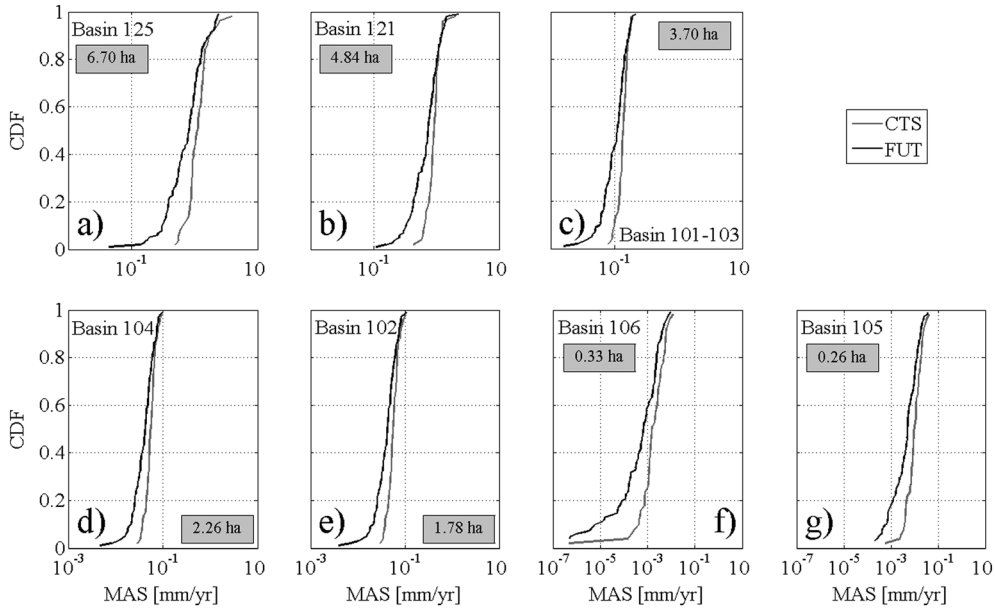

Figure 8. The cumulative frequency distributions of 30 year mean annual sediment yield (MAS) for the control (CTS, 50 realizations) and future (FUT, 100 realizations) climate ensembles. The results are presented for all seven basins arranged in the order corresponding to a decreasing area. The text in the grey boxes indicates the area of the basin expressed in hectares.

When the annual sediment yield per unit area for individual years is considered (i.e., not averaged over 30 years), the non-exceedance probability of sediment yield for the FUT set appears to be always higher than that for the CTS set (Figure 9). The differences in the probability of non-exceedance are remarkable especially during years with very low sediment yields (Figure 9). One can also notice that the probability of not having sediment yield in a given year increases considerably for the smaller basins. For instance, despite

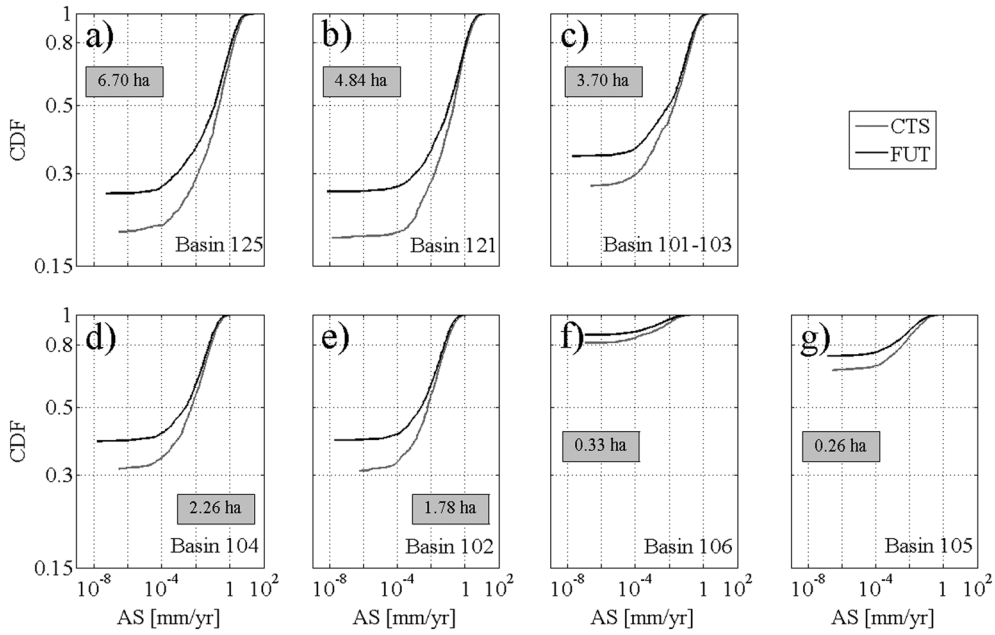

Figure 9. The cumulative frequency distributions of annual sediment yield, AS, for the control, CTS (50 scenarios, 30 year long each, or 1500 of simulated years in total), and future, FUT (100 scenarios, 30 year long each, or 3000 of simulated years in total), climate ensembles. Note that the distributions start at high values of the non-exceedance probability signifying the fraction of years with zero annual yield. The text in the grey boxes indicates the area of the basin expressed in hectares.

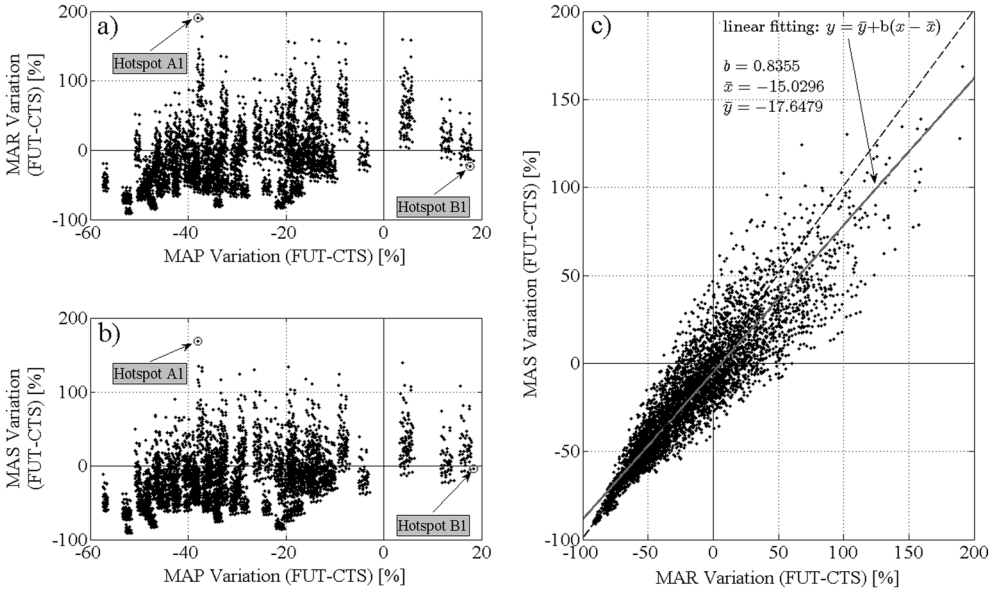

Figure 10. Relationships between variations in MAP, MAR, and MAS for Basin 101-103. The *x* axis in Figures 10a and 10b shows the change in precipitation calculated as the difference between each MAP member of the FUT ensemble and each member of the CTS scenario and normalized by dividing by MAP of the CTS member (in total, $100 \times 50 = 5000$ differences are computed). The *y* axis illustrates the corresponding normalized changes of (a) MAR and (b) MAS. These are similarly calculated as the difference between metric magnitudes of respective members in the FUT and CTS ensembles and normalized by the metric magnitude of the CTS member. (c) Relationship between the normalized changes in runoff and sediment yield shown in Figures 10a and 10b. The regression line between the changes in MAR and MAS, calculated with the principal axis regression method, has a slope equal to 0.8355. The black dashed line represents the 1 : 1 relationship.

the same rainfall and similar annual hydrologic response, Basins 105 and 106, for their size, exhibit a much higher probability to have years with no sediment yield, as compared to the rest of the study catchments.

4.4. Bivariate Analysis of Changes in Hydrologic and Geomorphologic Responses

A comparison of CDFs of MAR and MAS implies that despite a non-negligible probability of runoff increase in the projected future conditions (Figure 6), sediment yield exhibits a tendency to be always smaller than that in the present conditions (Figure 8). In order to elucidate this counterintuitive inference, we analyzed the interdependence between runoff and sediment yield, probabilistically characterizing their projected changes as functions of changes in rainfall. As a representative example for the study watersheds, the results are presented for Basin 101-103 (Figure 10). In Figure 10, the changes in MAP, MAR, and MAS are calculated as the difference between metric magnitudes of respective members in the FUT and CTS ensembles and normalized by the metric magnitude of the CTS member (in total, $100 \times 50 = 5000$ differences are computed). As seen, most of the points representing a relationship between variations in MAP, MAR, and MAS are in the third quadrant (Figures 10a–10c), where reductions in MAR and in MAS in the future correspond to a reduction in MAP (Figures 10a and 10b). The remaining points are scattered in the other quadrants with individual "hot spots": for example, the hot spot A1 is representative of a reduction in MAP but an increase in MAR and MAS, while the hot spot B1 is representative of an increase in MAP but a reduction in MAR and MAS. The different responses represented by these points are due to differences in rainfall characteristics. As an example, the hot spot A1 is due to the response of the basin to simulations with MAP of 302 mm/yr (CTS) and 187 mm/yr (FUT). Despite larger annual magnitude, the CTS ensemble member exhibits, on average, low rainfall intensities and a high number of rainfall events, as compared to the scenario characterizing future conditions. Larger average annual rainfall but lower individual event intensities of the CTS ensemble member thus result in smaller MAR and MAS, as compared to the FUT ensemble member that exhibits more intense rainfall. Conversely, the hot spot B1 is due to the response of the basin to MAP of about 296 and 348 mm/yr for the CTS and FUT scenarios, respectively, with the CTS intra-annual rainfall that, on average, exhibits slightly higher intensities and a lower number of events. In this case, the higher MAP of FUT ensemble member is insufficient to compensate for smaller intensities and the higher rainfall intensities of the CTS

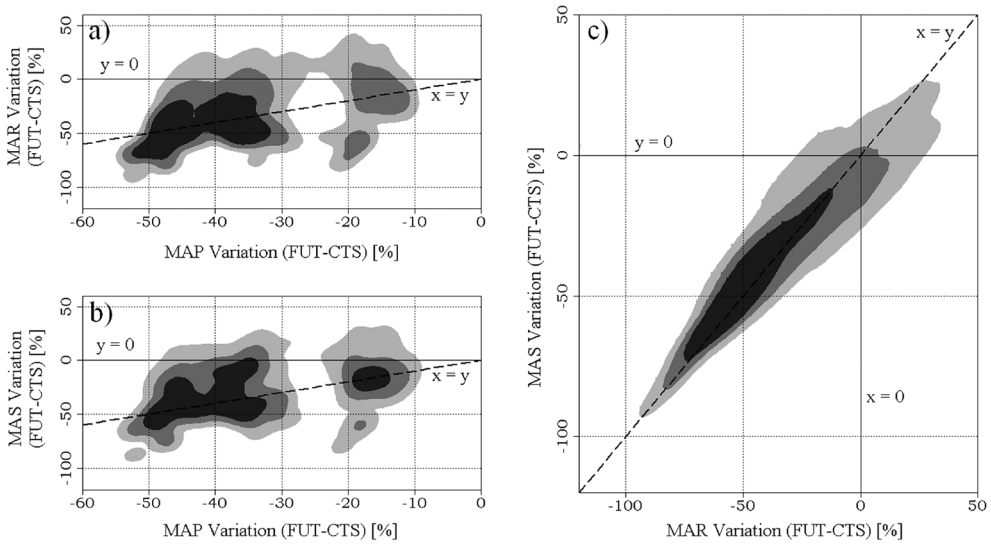

Figure 11. The Multivariate Kernel Density Estimation of the normalized changes in (a) MAP and MAR, (b) MAP and MAS, and (c) MAR and MAS for Basin 101-103; black = 25%, dark grey + black = 50%, light grey + dark grey + black = 75% of the bivariate distributions mass. The estimation function automatically selects an optimal bandwidth matrix (affects the performance of MKDE). The regression line between the changes in MAR and MAS has a slope equal to 0.8355. The black lines represent the 1 : 1 relationship.

scenario lead to relatively negligible differences between the FUT and the CTS in terms of runoff and sediment yield. When changes in MAR and MAS are simultaneously considered (Figure 10c), one may notice that the points are somewhat asymmetric with respect to the first bisector (Figure 10c). However, the fit line between the changes in MAR and MAS and calculated with the principal axis regression method is not 1 : 1 but has a slope equal to 0.8355 and a negative *y* intercept equal to −5.0908. This indicates that a probable future characterized by a decrease (increase) in runoff leads to less strongly decreased (increased) sediment yield. Moreover, the negative *y* intercept implies a probability that an increase in future runoff may lead to a decrease in sediment yield (points in the fourth quadrant).

In order to provide an assessment of probability for the joint variations of these variables, bivariate frequency distributions for changes in MAP and MAR (Figure 11a), MAP and MAS (Figure 11b), and MAR and MAS (Figure 11c) were estimated with the *Multivariate Kernel Density Estimation* (MKDE [*Simonoff*, 1996]), a nonparametric technique for estimation of probability density functions. MKDE is carried out using the kernel smoothing (*ks*) package of the statistical software R (version 2.15.3, 2013). For a given value of the normalized change in MAP, one can obtain a conditional probability density function (PDF) of the normalized changes in MAR (Figure 11a) and/or in MAS (Figure 11b). As seen, the area with the higher probability mass is mostly included in the third quadrant; this corresponds to a variation of MAP between −52% and −32% and a MAR variation between −70% and −15% (Figure 11a).

When changes in MAS are considered (Figure 11b), the area with the higher probability mass is still contained in the third quadrant but split into two regions. The first one corresponds to normalized changes of MAP between −51% and −33% and MAS variations between −60% and 0%; the second region corresponds to MAP variations between −20% and −15% and MAS variations between −25% and −10%. In both cases, almost half of the mass of the bivariate distribution is contained in the third quadrant, and 75% of the mass is within the second and third quadrants. This result is also reflected in the bivariate PDF of normalized changes in MAR and MAS: most of the mass is contained in the third quadrant (Figure 11c). In particular, the area corresponding to 25% of the mass (the black region) is entirely contained within the third quadrant. Note a non-negligible mass of the probability distribution in the fourth quadrant: it is representative of cases in which an increase in average runoff does not lead to an increase in sediment yield.

The results presented in Figures 10 and 11 can be considered to be representative of the Basins 102, 104, 121, and 125. However, the smaller Basins 105 and 106, although demonstrating qualitatively similar bivariate

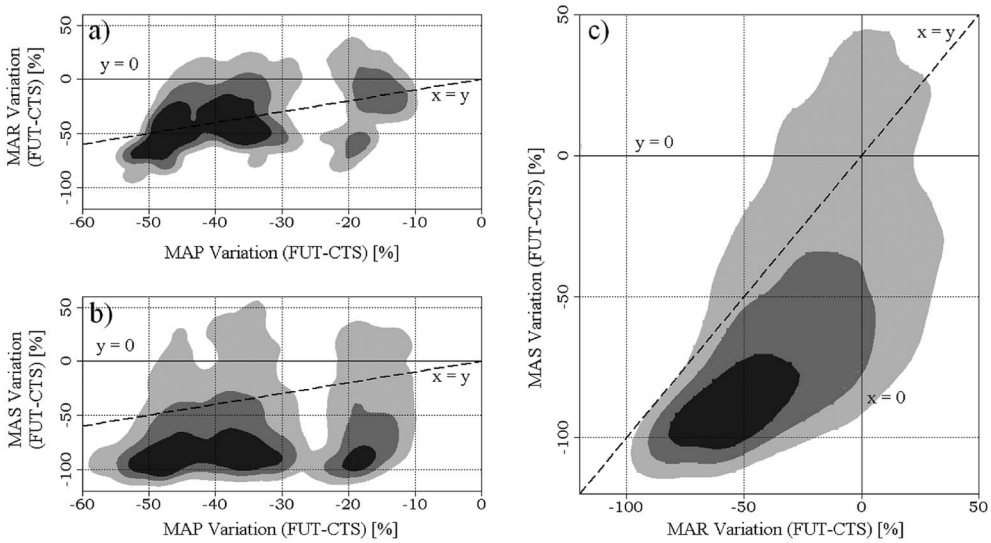

Figure 12. The Multivariate Kernel Density Estimation of the normalized changes in (a) MAP and MAR, (b) MAP and MAS, and (c) MAR and MAS for Basin 105; black = 25%, dark grey + black = 50%, light grey + dark grey + black = 75% of the bivariate distributions mass. The estimation function automatically selects an optimal bandwidth matrix (affects the performance of MKDE). The regression line between the changes in MAR and MAS, calculated with the principal axis regression method, has a slope equal to 2.7699. The black dashed lines represent the 1 : 1 relationship.

frequency distributions for variations in MAP and MAR (Figure 12a), show much higher variability in MAS (Figures 12b and 12c), as compared to the other basins (the results for Basin 105 are also representative for Basin 106). The fit line between the changes in MAR and MAS is steeper than that of Basin 101-103 and has a positive *y* intercept. The slope of the fit line greater than 1 indicates that, conversely to larger basins, a future characterized by a decrease (increase) in runoff may lead to an even stronger decrease (increase) in sediment yield. However, the spread over the *y* axis (Figure 12c) is larger, indicating a higher variability of changes in sediment transport, as compared to the other basins. The much higher variability in MAS of smaller basins suggests that the sediment transport response in these basins depends on local geomorphologic characteristics to a greater extent than the hydrological response.

4.5. Changes in Extremes

Runoff and sediment yield extremes, computed with the plotting-position method using annual maxima [*Cunnane*, 1978], were analyzed in order to explore the propagation of changes in extreme rainfall events to extreme sediment delivery events. Figure 13 synthesizes this information for Basin 101-103 and can be considered representative for the remaining basins. Changes in runoff extremes for the durations of 1 and 24 h (Figure 13) mostly reflect changes in rainfall extremes for the same time aggregation (Figures 4a and 4d). We only present the results for 1 and 24 h aggregation periods because the properties of runoff and sediment delivery responses are very similar also for durations of 3 and 6 h. In reference to the median of the stochastic ensemble, extreme events of sediment production are consistently projected to be smaller in the future, as a consequence of the decrease of runoff. However, the decrease in the median sediment transport (−15/−30%) for the higher return periods (>5 years) is typically larger than the projected change in the median runoff (−2/−16%) for the exemplary basins (see Table 2 for actual magnitudes). "Geomorphic multipliers" [*Coulthard et al.,* 2012], i.e., an enhanced decrease or increase of runoff and sediment delivery for larger return periods, are not clearly discernible in our analysis at the hourly scale, since changes for 5, 10, and 30 year return periods are rather similar for runoff and sediment yield (Table 2). One however can infer that the relative decrease of extreme runoff at the hourly scale is not accompanied by an equivalent change at the daily scale, following the pattern of projected changes in extreme rainfall. At the daily scale, the reduction of runoff is smaller than 8%, but changes in sediment yield are amplified (15–30%). This is because extreme sediment transport events are driven by runoff corresponding to event scale (i.e., shorter than the daily scale), which exhibits larger projected changes and comparable to what is illustrated for the duration of 1 h. More generally, Figure 13 suggests the dominance of uncertainty in the changes of extreme runoff and

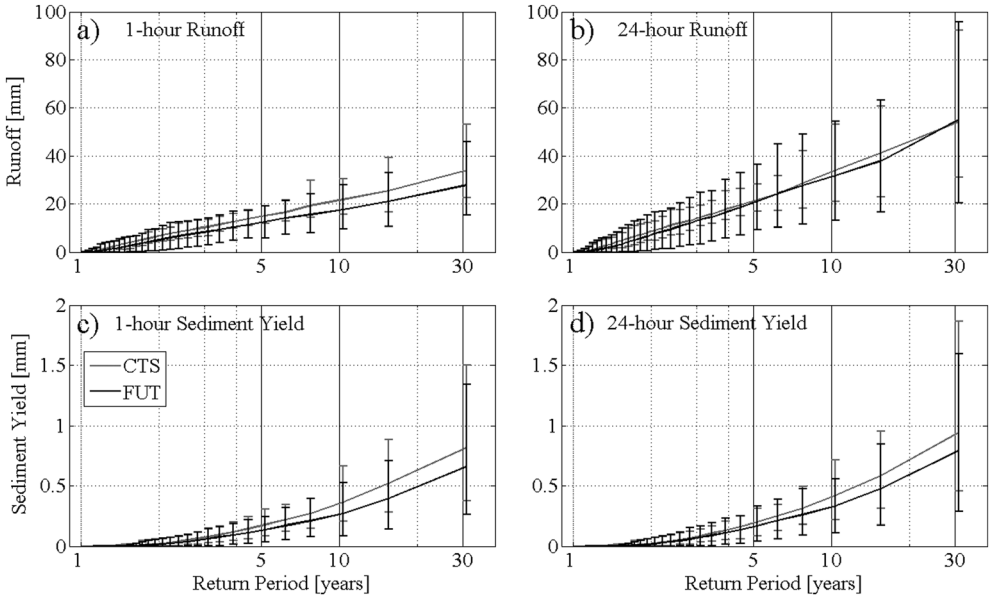

Figure 13. Changes in (a and b) extreme runoff and (c and d) sediment yield events for 1 (Figures 13a and 13c) and 24 h (Figures 13b and 13d) aggregation intervals. Extremes are computed from annual maxima and probabilities are assigned with the plotting-position method. Vertical bars denote the 5th to 95th percentiles of the CTS and FUT ensembles. The presented case is for the basin 101-103.

sediment transport events due to the stochastic variability of climate. The uncertainty range exhibits a large overlap between the CTS and the FUT scenarios, even though the latter are representative of 100 possible different climates, while the former represents only the present climate.

4.6. Scaling Relationships of Runoff and Sediment Yield

Results presented in section 4.4 suggest that differences in sediment yield and hydrological response of a basin may partially depend on its geomorphological characteristics. In order to investigate the possible dependence of these variables on the basin area, the scaling regime of runoff (Figure 14a) and sediment flux (Figure 14b) with watershed area is investigated. The modeled results, despite underestimation of runoff and

Table 2. Changes in Extreme Rain, Runoff, and Sediment Yield for 1 and 24 h Aggregation Intervals

			Basin 101-103			Basin 125		
Duration (h)	Variable (mm)	Return Period (years)	CTS (mm)	FUT (mm)	Δ(FUT − CTS) (%)	CTS (mm)	FUT (mm)	Δ(FUT − CTS) (%)
1	Rain	5	28.80	24.67	*−14.33*	28.80	24.67	*−14.33*
		10	33.10	28.79	*−13.04*	33.10	28.79	*−13.04*
		30	43.75	36.98	*−15.48*	43.75	36.98	*−15.48*
	Runoff	5	15.01	12.46	*−16.98*	14.70	12.06	*−17.98*
		10	21.89	17.51	*−19.99*	21.15	16.88	*−20.20*
		30	34.02	27.77	*−18.39*	33.32	26.74	*−19.73*
	Sediment yield	5	0.18	0.14	*−22.71*	1.40	0.98	*−29.94*
		10	0.37	0.27	*−26.09*	2.89	2.06	*−28.77*
		30	0.82	0.66	*−19.38*	9.41	5.79	*−38.52*
24	Rain	5	53.25	52.86	*−0.73*	53.25	52.86	*−0.73*
		10	64.68	65.65	*1.51*	64.68	65.65	*1.51*
		30	85.56	87.35	*2.09*	85.56	87.35	*2.09*
	Runoff	5	21.62	21.10	*−2.42*	21.01	20.09	*−4.37*
		10	33.98	31.78	*−6.48*	33.18	30.54	*−7.94*
		30	54.15	55.09	*1.74*	52.51	51.17	*−2.54*
	Sediment yield	5	0.20	0.17	*−15.89*	1.62	1.23	*−23.91*
		10	0.42	0.33	*−20.46*	3.25	2.40	*−26.10*
		30	0.95	0.79	*−16.07*	9.96	6.99	*−29.84*

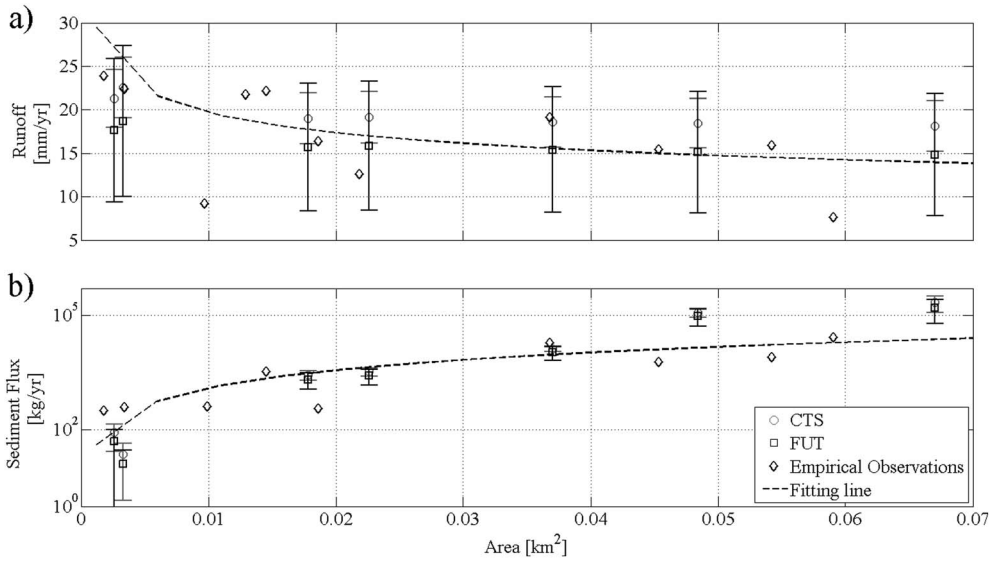

Figure 14. Scaling relationships for (a) mean annual runoff and (b) sediment flux with area. The black diamonds represent empirical observations and the black dashed line is the corresponding fit that follows *Stone et al.* [2008] for runoff and *Nichols et al.* [2008] for the sediment yield. The grey circles and the black squares error bars correspond to the results obtained for the CTS and the FUT ensembles, respectively. The confidence bounds represent standard deviations estimated using the ensemble members (50 for CTS and 100 for FUT).

sediment yield for the smaller basins and overestimation of sediment yield for the larger basins, do reproduce the major characteristics of runoff and sediment yield scaling with the contributing area. Regardless of the larger uncertainty characteristic of the FUT climate (i.e., larger error bars), no detectable changes in the scaling, but rather a reduction of the magnitudes of sediment yield and runoff can be observed.

A statistical assessment of changes in the fit of the scaling relationship obtained for the current climate in the form of a power law model, $y = ax^b$, is carried out for both mean annual runoff and sediment yield. Simulation results for the CTS and FUT were used to fit the relationship versus area, where y is runoff (or sediment yield) and x is the basin area. The intercept, a, and the slope, b, of the power law are not significantly different between the CTS and FUT scenarios for the sediment yield (analysis of covariance test with the 0.05 significance level). The slope of the scaling relationship for runoff is still not significant (p value = 0.838, the null hypothesis of equal slopes), while the intercept is significantly different, which means lower runoff with the same scaling exponent (Table 3).

Table 3. Statistical Assessment of Difference From the Fits Obtained for the Scaling Relationships of Current and Future Climate of Runoff and Sediment Yield[a]

		Runoff (mm/yr)		Sediment Yield (kg/yr)	
Ensemble		CTS	FUT	CTS	FUT
Fitting model				ax^b	
Coefficients	a	15.16	12.4	3.81×10^8	1.72×10^8
	b	−0.06224	−0.0645	2.763	2.582
95% Confidence bounds	a	13.62–16.7	11.17–13.63	-9.885×10^8 to 1.75×10^9	-5.032×10^8 to 8.467×10^8
	b	−0.08517 to −0.0393	−0.08688 to −0.04213	1.466–4.059	1.171–3.993
ANCOVA (p value)	a	0.0		0.4943	
	b	0.8382		0.8031	
SSE		1.624	1.056	1.78×10^9	1.36×10^9
R^2		0.9037	0.9138	0.9571	0.9409
Adjusted R^2		0.8844	0.8966	0.9485	0.9291
RMSE		0.5699	0.4596	1.886×10^4	1.648×10^4

[a]ANCOVA, analysis of covariance for difference between future and present; SSE, sum of squares due to error; R^2, R-square; Adjusted R^2, degrees of freedom adjusted R-square; RMSE, root mean squared error.

5. Discussion

5.1. Projected Changes and Mechanistic Interpretation

Based on stochastic downscaling of climate projections for the study location in southeastern Arizona, USA, annual precipitation is generally expected to decrease in the future (Figure 2a), with rainfall events characterized, on average, by lower intensities at the hourly scale, as compared to the present climate (Figure 3a). Furthermore, when medians of extreme rainfall are analyzed, future climate is characterized by less extreme events at the hourly scale than the present climate but of similar average intensity at the daily scale (even though these results exhibit a large uncertainty; Figure 4a).

The lower hourly rainfall (across all percentile ranges) results in generally lower mean annual runoff in the future, as compared to historic conditions. However, 15–20% of the stochastic ensemble members show that 30 year averaged runoff could be higher in the future conditions (Figures 6 and 7). This result demonstrates that runoff behaves nonlinearly and differently than stochastically driven precipitation, whose mean in the FUT scenarios is expected to be nearly always lower than the mean representative of the historic period (CTS scenarios; Figure 2a).

A non-negligible chance of runoff increase in the future is a consequence of stochastic combinations of years with low and high runoff due to interannual variability, rather than an emergence of alternative futures with years characterized by exceptionally high runoff. A more in-depth explanation has to relate to the predominant physical mechanism of runoff generation in the analyzed area—the infiltration excess process. Specifically, since total precipitation is projected to decrease, hypothetically, higher runoff in the future can result either from a larger number of rainfall events within a year exceeding temporally dynamic threshold of infiltration capacity or merely from a combination of years in the FUT and CTS ensembles (i.e., interannual variability in the ensemble member). Since the annual runoff projected for all percentiles corresponds to magnitudes lower than that in the control period, the former possibility is not the case (Figure 7). Therefore, the only explanation of larger runoff in the future is the composition of 30 year ensemble members: a combination of years with relatively high runoff magnitudes may result in larger 30 year runoff averages, as compared to the CTS scenario (Figure 6).

On average, the mean sediment yield is expected to decrease in the future with a very high probability (Figures 8 and 9). Moreover, for all of the basins, the predicted variability (i.e., the standard deviation over a 30 year period of a single climate realization) for the future conditions as well as extreme sediment transport events is comparable to that for the present conditions. This is despite the fact that the future scenarios account for a much wider range of possible climates that are "sampled" from the distributions of factors of change. This is a very significant result that shows how natural climate variability, i.e., stochasticity, in the present plays a progressively more important role when rainfall, runoff, and sediment yield are successively analyzed. Fundamentally, the stochastic variability of sediment yield corresponding to the present climate (i.e., a single, stationary climate) is already so high, that it is "comparable" to the variability induced by considering multiple possible future climates due to uncertainty of projections. This also highlights that a simple evaluation of sediment transport characteristics for the present climate should be carried out in a stochastic framework, where a single realization (i.e., that can be derived from observational record [e.g., *Nearing et al.*, 2008; *Polyakov et al.*, 2010]) can be only partially informative of the current conditions [see also *Coulthard et al.*, 2012]. We also remark that it is quite unrealistic for studies based on observed trends and comparisons with a single or a few deterministic future scenarios to obtain meaningful results, because of the significant stochastic variability of extreme events that are the primary drivers for runoff and sediment transport events in semiarid environments. Note that the stochastic variability may not only be climate induced but could be also governed by hydrologic and geomorphic initial conditions anteceding the events [*Kim and Ivanov*, 2014], although this is not addressed here.

As inferred from empirical observations, sediment flux in absolute units exhibits a positive dependence on basin area (Figure 14b). Consistently, this relationship is a result of the larger area that leads to higher rates of concentrated runoff and transport capacities that have a greater chance of exceeding entrainment threshold (i.e., the critical shear stress). The variability induced by climate in erosion and sediment transport variables can be amplified or dampened by basin geomorphic characteristics. For example, for smaller watersheds, where thresholds for particle detachment and transport capacity are less likely to be exceeded, as compared to larger basins, the probability of not having sediment flux in a given year increases

considerably (Figure 9). We note however that since vegetation is sparse and parameterized to have little canopy (Table S1 in the supporting information), a thresholding effect in the detachment erosion is overall of minor significance and detachment capacity scales as a power law function with rainfall magnitude [*Francipane et al.,* 2012].

The differences of responses of runoff and sediment yield that we reveal in this study, i.e., the 15–20% chance of higher future runoff, while the zero chance of higher future sediment yield, can be attributed to the nature of physical processes governing erosion and sediment transport in the analyzed watersheds. Runoff is exclusively generated through the infiltration excess mechanism and the process is confined to most intense storms. Erosion and sediment transport are triggered only by a fraction of runoff events that are most extreme and have short durations, coinciding with the timing of runoff peak (1–2 h). This is because the critical shear stress in entrainment and transport capacities has to be exceeded before flowing water can transport soil particles, making the occurrence of these processes infrequent, especially in smaller watersheds. Many simulated years exhibit sediment yield close or equal to 0, despite runoff-generating events (Figures 7 and 9). Therefore, while changes in precipitation interannual variability lead to potential futures with an increase in runoff, they do not affect in the same fashion sediment yield, because subdaily rainfall is projected to decrease in intensity or remain within the range of stochastic variability characterizing the historic conditions (Figures 3 and 4). At these subdaily scales, median hourly runoff and sediment transport extremes are both projected to decrease (Figures 13a and 13c), as the chance that surface flow exceeds the rate required for effective particle entrainment also goes down. However, such an agreement between projections for runoff and sediment yield is lost at the 24 h aggregation interval, at which median extreme runoff is essentially projected to remain unchanged, while sediment yield still decreases (Figures 13b and 13d). This is because the exceedance of the transport capacity threshold that results in sediment transport events is mainly controlled by characteristics of shorter temporal scales (e.g., hourly peak runoff), i.e., the same daily runoff in the projected future but composed of events of smaller magnitude necessarily leads to a reduction in daily sediment.

We also investigated how climate change affects properties of extreme events (Figure 13) and scaling relationships of runoff and specific sediment yield with the watershed drainage area (Figure 14). We find that the concept of "geomorphic multipliers" [*Coulthard et al.,* 2012], i.e., a much stronger decrease or increase of sediment yield, as compared to runoff, for larger return periods, is still valid at the daily or coarser temporal aggregations (Table 2). This is not the case for the hourly scale, at which similar reductions in runoff and sediment yield are exhibited for different return periods and with larger uncertainties (Table 2). Despite the overall projection of decreases in runoff and sediment yield, we did not find any evidence for changes in scaling regimes of runoff and sediment yield with contributing area. The intercepts, rather than the exponents, of these relationships are mostly affected by the climate change (a statistically significant change in the intercept for runoff), even though large uncertainties induced by the stochastic variability preclude robust conclusions.

5.2. Limits of Interpretation and Stochastic Variability

There are certain limitations to the approach undertaken in this study. The Walnut Gulch area is located in a semiarid region characterized by highly seasonal rainfall dominated by summer monsoon, with localized, spatially variable, high-intensity storms. The presented results are therefore likely to be valid only for headwater catchments in semiarid climatic conditions and for climate projections showing a reduction or unchanged mean precipitation and extreme rainfall events. The paramount importance of short temporal scales for sediment generation hints that despite the fact that we used hourly resolution and could reproduce well extreme events, rainfall variability at the subhourly scale may be still important for addressing climatic impacts in this type of environment, where storms of highest intensity can last less than 1 h [*Osborn*, 1983]. Another important control of sediment dynamics, such as the effects of vegetation dynamics on erosion activity (growth and death of vegetation, feedbacks, and seasonal cycles due to climate and/or erosion/deposition events), is not investigated in this study. The uncertainty of parameters controlling sediment transport is also not explicitly analyzed: the parameter values were inherited from the long-term calibration and validation carried out for the Lucky Hills basin in *Francipane et al.* [2012]. High spatial variability of hydraulic and hydrologic properties known from empirical observations is another source of uncertainty that can exhibit the property of amplifying or dampening the projection assessment. It warrants a comprehensive approach and a separate

study and thus was also not addressed here. Additionally, this study considered only a single climate change projection, the A1B gas emission scenario, which limits broader interpretation of the results in the context of uncertainties of climate scenarios.

Despite these limitations, some of the results are likely to be of general applicability for projecting climate change impacts in semiarid watersheds. The role of changes in precipitation from the hourly to the annual scales has been found to be predominant, with the compounding effect of basin size being of secondary importance. Admittedly, the range of analyzed basin areas is fairly limited and the role of watershed shape, slope, and morphology is not explicitly considered. Importantly, the finding that we believe to be very general concerns the importance of the stochastic variability. Any assessment of long-term sediment yield is subject to uncertainty because of dependence of erosion physical processes on short-term (subhourly to few hours) characteristics of stochastic process of rainfall; the uncertainty corresponding to historic climate conditions is very high and is comparable to that inferred for future conditions that are subject to projection uncertainties.

Consistently with the above inference, the approach undertaken assumes deterministic simulations within a stochastic framework (and thus follows the same philosophical strategy as the study of *Coulthard et al.* [2012]). We believe it represents the only consistent approach for assessment of hydrogeomorphic changes that are controlled by extreme, rare events. Changes in runoff and sediment yield extremes show an amplification/dampening effect when rainfall, discharge, and sediment transport are successively analyzed. Extremes cannot be well characterized by using only limited observational data because of the intrinsic natural variability of climate and because of nonlinearity imposed by thresholds in underlying physical processes (infiltration capacity and transport capacities in our case). Therefore, a proper characterization of hydrogeomorphic variables necessitates taking into account both the variability of the historic conditions as well as the uncertainties associated with projections of the future. Only in this case, i.e., when a comprehensive probabilistic framework is developed, we can rationally address impending challenges of the climate change and design mitigation strategies.

6. Conclusions

Runoff, erosion, and sediment transport were simulated for seven headwater catchments located in a semiarid environment of southeast Arizona. We used a mechanistic, process-based hydrogeomorphic model forced with multiple climate conditions representative of the present and projected future climates. A stochastic approach is used to assess probable changes in precipitation, runoff, and sediment yield. An overall reduction in precipitation mean and hourly intensities leads to a concurrent decrease in runoff and sediment yield. Increases in long-term runoff not accompanied by larger sediment delivery are also projected for some scenarios, as a consequence of changes in interannual variability of precipitation. Intense runoff events of short duration (<2 h) that lead to exceedance of thresholds in soil detachment/entrainment and transport capacities are the major controllers of sediment yield. Changes in the occurrence of these extreme events are subject to a very large uncertainty due to the natural climate variability. As the study finds, current stochastic variability in erosion events is almost comparable to that projected for multiple future climate alternatives. The importance of stochastic variability is shown to grow when rainfall, runoff, and sediment yield are successively analyzed. Ultimately, this leads to a conclusion that climate change effects on sediment transport cannot be properly addressed without understanding of stochastic variability representative of historic conditions as well as climate model and stochastic uncertainties associated with projected future conditions.

Acknowledgments
We acknowledge the modeling groups, the Program for Climate Model Diagnosis and Intercomparison (PCMDI) and the WCRP's Working Group on Coupled Modeling (WGCM) for their roles in making available the WCRP CMIP3 multimodel data set. Support of this data set is provided by the Office of Science, U.S. Department of Energy. Ivanov is supported by the NSF grant EAR 1151443 and partially by the Visiting Faculty grant at the Institute of Environmental Engineering, ETH Zürich. Francipane and Noto were supported by the SESAMO (*SistEma informativo integrato per l'acquisizione, geStione e condivisione di dAti aMbientali per il suppOrto alle decisioni* project. Authors would like to acknowledge helpful criticism of T. Coulthard, G. Tucker, and three other anonymous reviewers that substantially improved the quality of this manuscript.

References

Anandhi, A., A. Frei, D. C. Pierson, E. M. Schneiderman, M. S. Zion, D. Lounsbury, and A. H. Matonse (2011), Examination of change factor methodologies for climate change impact assessment, *Water Resour. Res.*, *47*, W03501, doi:10.1029/2010WR009104.

Birkinshaw, S. J., and J. C. Bathurst (2006), Model study of the relationship between sediment yield and river basin area, *Earth Surf. Processes Landforms*, *31*(6), 750–761, doi:10.1002/Esp.1291.

Chaplot, V. (2007), Water and soil resources response to rising levels of atmospheric CO_2 concentration and to changes in precipitation and air temperature, *J. Hydrol.*, *337*(1–2), 159–171, doi:10.1016/j.jhydrol.2007.01.026.

Chen, J., F. P. Brissette, and R. Leconte (2011), Uncertainty of downscaling method in quantifying the impact of climate change on hydrology, *J. Hydrol.*, *401*(3–4), 190–202, doi:10.1016/j.jhydrol.2011.02.020.

Christensen, J. H., et al. (2007), *Regional Climate Projections, Climate Change, 2007: The Physical Science Basis. Contribution of Working Group I to the Fourth Assessment Report of the Intergovernmental Panel on Climate Change*, edited by S. Solomon et al., p. 996, Cambridge Univ. Press, Cambridge, U. K.

Coppus, R., and A. C. Imeson (2002), Extreme events controlling erosion and sediment transport in a semi-arid sub-Andean valley, *Earth Surf. Processes Landforms*, *27*(13), 1365–1375, doi:10.1002/esp.435.
Coulthard, T. J., and M. G. Macklin (2001), How sensitive are river systems to climate and land-use changes? A model-based evaluation, *J. Quat. Sci.*, *16*(4), 347–351, doi:10.1002/jqs.604.
Coulthard, T. J., M. G. Macklin, and M. J. Kirkby (2002), A cellular model of Holocene upland river basin and alluvial fan evolution, *Earth Surf. Processes Landforms*, *27*(3), 269–288, doi:10.1002/Esp.318.
Coulthard, T. J., J. Lewin, and M. G. Macklin (2005), Modelling differential catchment response to environmental change, *Geomorphology*, *69*(1–4), 222–241, doi:10.1016/j.geomorph.2005.01.008.
Coulthard, T. J., J. Ramirez, H. J. Fowler, and V. Glenis (2012), Using the UKCP09 probabilistic scenarios to model the amplified impact of climate change on drainage basin sediment yield, *Hydrol. Earth Syst. Sci.*, *16*(11), 4401–4416, doi:10.5194/hess-16-4401-2012.
Cowpertwait, P., V. Isham, and C. Onof (2007), *Point Process Models of Rainfall: Developments for Fine-Scale Structure*, pp. 2569–2587.
Cowpertwait, P. S. P. (1991), Further developments of the neyman-scott clustered point process for modeling rainfall, *Water Resour. Res.*, *27*(7), 1431–1438, doi:10.1029/91WR00479.
Cowpertwait, P. S. P., P. E. O'Connell, A. V. Metcalfe, and J. A. Mawdsley (1996), Stochastic point process modelling of rainfall. I. Single-site fitting and validation, *J. Hydrol.*, *175*(1–4), 17–46, doi:10.1016/S0022-1694(96)80004-7.
Cunnane, C. (1978), Unbiased plotting positions — A review, *J. Hydrol.*, *37*(3-4), 205–222, doi:10.1016/0022-1694(78)90017-3.
De Boer, D. H., and G. Crosby (1996), *Specific Sediment Yield and Drainage Basin Scale, Paper Presented at Global and Regional Perspective*, IAHS, Exeter, U. K.
Dedkov, A. (2004), The relationship between sediment yield and drainage basin area, in *Sediment Transfer Through the Fluvial System: Proceedings of the International Symposium Held at Moscow, Russia, from 2 to 6 August, 2004*, pp. 197–204, IAHS, Wallingford, U. K.
Deser, C., A. Phillips, V. Bourdette, and H. Y. Teng (2012a), Uncertainty in climate change projections: The role of internal variability, *Clim. Dyn.*, *38*(3–4), 527–546, doi:10.1007/s00382-010-0977-x.
Deser, C., R. Knutti, S. Solomon, and A. S. Phillips (2012b), Communication of the role of natural variability in future North American climate, *Nat. Clim. Change*, *2*(11), 775–779, doi:10.1038/Nclimate1562.
de Vente, J., J. Poesen, M. Arabkhedri, and G. Verstraeten (2007), The sediment delivery problem revisited, *Prog. Phys. Geogr.*, *31*(2), 155–178, doi:10.1177/0309133307076485.
Easterling, D. R., G. A. Meehl, C. Parmesan, S. A. Changnon, T. R. Karl, and L. O. Mearns (2000), Climate extremes: Observations, modeling, and impacts, *Science*, *289*(5487), 2068–2074, doi:10.1126/science.289.5487.2068.
Emmerich, W. E., and C. L. Verdugo (2008), Long-term carbon dioxide and water flux database, Walnut Gulch Experimental Watershed, Arizona, United States, *Water Resour. Res.*, *44*, W05S09, doi:10.1029/2006WR005693.
Enke, W., and A. Spekat (1997), Downscaling climate model outputs into local and regional weather elements by classification and regression, *Clim. Res.*, *8*(3), 195–207, doi:10.3354/cr008195.
Enke, W., T. Deutschlander, F. Schneider, and W. Kuchler (2005), Results of five regional climate studies applying a weather pattern based downscaling method to ECHAM4 climate simulations, *Meteorol. Z.*, *14*(2), 247–257, doi:10.1127/0941-2948/2005/0028.
Entekhabi, D. (2000), *Land Surface Processes: Basic Tools and Concepts*, MIT, Cambridge, Mass.
Fatichi, S. (2010), The modeling of hydrological cycle and its interaction with vegetation in the framework of climate change, PhD dissertation thesis, Univ. of Firenze and T.U. Braunschweig.
Fatichi, S., V. Y. Ivanov, and E. Caporali (2011), Simulation of future climate scenarios with a weather generator, *Adv. Water Resour.*, *34*(4), 448–467, doi:10.1016/j.advwatres.2010.12.013.
Fatichi, S., V. Y. Ivanov, and E. Caporali (2012), A mechanistic ecohydrological model to investigate complex interactions in cold and warm water-controlled environments: 2 Spatiotemporal analyses, *J. Adv. Model. Earth Syst.*, *4*, M05003, doi:10.1029/2011MS000087.
Fatichi, S., V. Y. Ivanov, and E. Caporali (2013), Assessment of a stochastic downscaling methodology in generating an ensemble of hourly future climate time series, *Clim. Dyn.*, *40*(7–8), 1841–1861, doi:10.1007/s00382-012-1627-2.
Fatichi, S., S. Rimkus, P. Burlando, and R. Bordoy (2014), Does internal climate variability overwhelm climate change signals in streamflow? The upper Po and Rhone basin case studies, *Sci. Total Environ.*, *493*, 1171–1182, doi: 10.1016/j.scitotenv.2013.12.014.
Favis-Mortlock, D., and J. Boardman (1995), Nonlinear responses of soil erosion to climate change: A modelling study on the UK South Downs, *Catena*, *25*(1–4), 365–387, doi:10.1016/0341-8162(95)00018-n.
Favis-Mortlock, D. T., and S. J. T. Guerra (1999), The implications of general circulation model estimates of rainfall for future erosion: A case study from Brazil, *Catena*, *37*(3–4), 329–354, doi:10.1016/S0341-8162(99)00025-9.
Favis-Mortlock, D. T., and M. R. Savabi (1996), Shifts in rates and spatial distribution of soil erosion and deposition under climate change, in *Advances in Hillslope Processes*, edited by M. G. Anderson and S. M. Brooks, pp. 129–560, John Wiley, New York.
Fischer, E. M., U. Beyerle, and R. Knutti (2013), Robust spatially aggregated projections of climate extremes, *Nat. Clim. Change*, *3*(12), 1033–1038, doi:10.1038/nclimate2051.
Flerchinger, G. N., W. P. Kustas, and M. A. Weltz (1998), Simulating surface energy fluxes and radiometric surface temperatures for two arid vegetation communities using the SHAW model, *J. Appl. Meteorol.*, *37*(5), 449–460, doi:10.1175/1520-0450(1998)037<0449:Ssefar>2.0.Co;2.
Fowler, A. M., and K. J. Hennessy (1995), Potential impacts of global warming on the frequency and magnitude of heavy precipitation, *Nat. Hazards*, *11*(3), 283–303, doi:10.1007/Bf00613411.
Francipane, A. (2010), tRIBS-Erosion: A physically-based model for studying mechanisms of eco-hydro-geomorphic coupling, PhD dissertation thesis, Univ. of Palermo, Palermo.
Francipane, A., V. Y. Ivanov, L. V. Noto, E. Istanbulluoglu, E. Arnone, and R. L. Bras (2012), tRIBS-Erosion: A parsimonious physically-based model for studying catchment hydro-geomorphic response, *Catena*, *92*, 216–231, doi:10.1016/j.catena.2011.10.005.
Freeze, R. A., and J. A. Cherry (1979), *Groundwater*, Prentice-Hall, Englewood Cliffs, N. J.
Goodrich, D. C., L. J. Lane, R. M. Shillito, S. N. Miller, K. H. Syed, and D. A. Woolhiser (1997), Linearity of basin response as a function of scale in a semiarid watershed, *Water Resour. Res.*, *33*(12), 2951–2965, doi:10.1029/97WR01422.
Goodrich, D. C., T. O. Keefer, C. L. Unkrich, M. H. Nichols, H. B. Osborn, J. J. Stone, and J. R. Smith (2008a), Long-term precipitation database, Walnut Gulch Experimental Watershed, Arizona, United States, *Water Resour. Res.*, *44*, W05S04, doi:10.1029/2006WR005782.
Goodrich, D. C., C. L. Unkrich, T. O. Keefer, M. H. Nichols, J. J. Stone, L. R. Levick, and R. L. Scott (2008b), Event to multidecadal persistence in rainfall and runoff in southeast Arizona, *Water Resour. Res.*, *44*, W05S14, doi:10.1029/2007WR006222.
Gueymard, C. A. (2008), REST2: High-performance solar radiation model for cloudless-sky irradiance, illuminance, and photosynthetically active radiation - Validation with a benchmark dataset, *Sol. Energy*, *82*(3), 272–285, doi:10.1016/j.solener.2007.04.008.

Hack, J. T., and J. C. Goodlett (1960), *Geomorphology and Forest Ecology of a Mountain Region in the Central Appalachians*, U. S. Gov. Print. Off., Washington D. C.
Hancock, G. R., and T. J. Coulthard (2012), Channel movement and erosion response to rainfall variability in southeast Australia, *Hydrol. Processes*, *26*(5), 663–673, doi:10.1002/Hyp.8166.
Hancock, G. R., T. J. Coulthard, and G. R. Willgoose (2011), Modeling erosion and channel movement - Response to rainfall variability in south east Australia, pp. 1874–1880.
Hawkins, E., and R. Sutton (2011), The potential to narrow uncertainty in projections of regional precipitation change, *Clim. Dyn.*, *37*(1–2), 407–418, doi:10.1007/s00382-010-0810-6.
Hu, Z., and S. Islam (1995), Prediction of ground surface temperature and soil moisture content by the force-restore method, *Water Resour. Res.*, *31*(10), 2531–2539, doi:10.1029/95WR01650.
Imeson, A. C., and H. Lavee (1998), Soil erosion and climate change: The transect approach and the influence of scale, *Geomorphology*, *23*(2–4), 219–227, doi:10.1016/S0169-555x(98)00005-1.
Intergovernmental Panel on Climate Change (2007), Summary for policymakers, in *Climate Change 2007: The Physical Science Basis. Contribution of Working Group I to the Fourth Assessment Report of the Intergovernmental Panel on Climate Change*, Cambridge Univ. Press, Cambridge, U. K., and New York.
Istanbulluoglu, E. (2009a), Modeling catchment evolution: From decoding geomorphic processes signatures toward predicting impacts of climate change, *Geogr. Compass*, *3*(3), 1125–1150, doi:10.1111/j.1749-8198.2009.00228.x.
Istanbulluoglu, E. (2009b), An eco-hydro-geomorphic perspective to modeling the role of climate in catchment evolution, *Geogr Compass*, *3*(3), 1151–1175, doi:10.1111/j.1749-8198.2009.00229.x.
Istanbulluoglu, E., and R. L. Bras (2005), Vegetation-modulated landscape evolution: Effects of vegetation on landscape processes, drainage density, and topography, *J. Geophys. Res.*, *110*, F02012, doi:10.1029/2004JF000249.
Istanbulluoglu, E., D. G. Tarboton, R. T. Pack, and C. H. Luce (2004), Modeling of the interactions between forest vegetation, disturbances, and sediment yields, *J. Geophys. Res.*, *109*, F01009, doi:10.1029/2003JF000041.
Ivanov, V. Y., E. R. Vivoni, R. L. Bras, and D. Entekhabi (2004a), Preserving high-resolution surface and rainfall data in operational-scale basin hydrology: A fully-distributed physically-based approach, *J. Hydrol.*, *298*(1–4), 80–111, doi:10.1016/j.jhydrol.2004.03.041.
Ivanov, V. Y., E. R. Vivoni, R. L. Bras, and D. Entekhabi (2004b), Catchment hydrologic response with a fully distributed triangulated irregular network model, *Water Resour. Res.*, *40*, W11102, doi:10.1029/2004WR003218.
Kim, J., and V. Y. Ivanov (2014), On the nonuniqueness of sediment yield at the catchment scale: The effects of soil antecedent conditions and surface shield, *Water Resour. Res.*, *50*, 1025–1045, doi:10.1002/2013wr014580.
Kim, J., V. Y. Ivanov, and N. D. Katopodes (2013), Modeling erosion and sedimentation coupled with hydrological and overland flow processes at the watershed scale, *Water Resour. Res.*, *49*, 5134–5154, doi:10.1002/wrcr.20373.
Kim, M. K., D. C. Flanagan, J. R. Frankenberger, and C. R. Meyer (2009), Impact of precipitation changes on runoff and soil erosion in Korea using CLIGEN and WEPP, *J. Soil Water Conserv.*, *64*(2), 154–162, doi:10.2489/jswc.64.2.154.
King, D. M., S. M. Skirvin, C. D. H. Collins, M. S. Moran, S. H. Biedenbender, M. R. Kidwell, M. A. Weltz, and A. Diaz-Gutierrez (2008), Assessing vegetation change temporally and spatially in southeastern Arizona, *Water Resour. Res.*, *44*, W05S15, doi:10.1029/2006WR005850.
Kunkel, K. E., D. R. Easterling, D. A. R. Kristovich, B. Gleason, L. Stoecker, and R. Smith (2010), Recent increases in U.S. heavy precipitation associated with tropical cyclones, *Geophys. Res. Lett.*, *37*, L24706, doi:10.1029/2010GL045164.
Laflen, J. M., L. J. Lane, and G. R. Foster (1991), WEPP: A new generation of erosion prediction technology, *J. Soil Water Conserv.*, *46*(1), 34–38.
Lane, S. N. (2013), 21st century climate change: Where has all the geomorphology gone?, *Earth Surf. Processes Landforms*, *38*(1), 106–110, doi:10.1002/esp.3362.
Langbein, W. B., and S. A. Schumm (1958), Yield of sediment in relation to mean annual precipitation, *Trans. Am. Geophys. Union*, *39*(6), 1076, doi:10.1029/TR039i006p01076.
Lin, J. D. (1980), On the force-restore method for prediction of ground surface temperature, *J. Geophys. Res.*, *85*(C6), 3251–3254, doi:10.1029/JC085iC06p03251.
Lu, H., C. J. Moran, and M. Sivapalan (2005), A theoretical exploration of catchment-scale sediment delivery, *Water Resour. Res.*, *41*, W09415, doi:10.1029/2005WR004018.
Martin, Y. E. (2013), 14.6 Methods in geomorphology: Numerical modeling of drainage basin development, in *Treatise on Geomorphology*, edited by J. F. Shroder, pp. 65–72, Academic Press, San Diego, Calif.
Martin, Y., and M. Church (2004), Numerical modelling of landscape evolution: Geomorphological perspectives, *Prog. Phys. Geogr.*, *28*(3), 317–339, doi:10.1191/0309133304pp412ra.
Meehl, G. A., C. Covey, T. Delworth, M. Latif, B. McAvaney, J. F. B. Mitchell, R. J. Stouffer, and K. E. Taylor (2007), The WCRP CMIP3 multimodel dataset - A new era in climate change research, *Bull. Am. Meteorol. Soc.*, *88*(9), 1383–1394, doi:10.1175/Bams-88-9-1383.
Monteith, J. L. (1965), Evaporation and environment, *Symp. Soc. Exp. Biol.*, *19*, 205–234.
Morris, G. L., and J. Fan (1998), *Reservoir Sedimentation Handbook*, McGraw-Hill Book Co., New York.
Mullan, D. (2013), Soil erosion under the impacts of future climate change: Assessing the statistical significance of future changes and the potential on-site and off-site problems, *Catena*, *109*, 234–246, doi:10.1016/j.catena.2013.03.007.
Mullan, D., D. Favis-Mortlock, and R. Fealy (2012), Addressing key limitations associated with modelling soil erosion under the impacts of future climate change, *Agric. For. Meteorol.*, *156*(0), 18–30, doi:10.1016/j.agrformet.2011.12.004.
Murphy, J. M., et al. (2009), UK climate projections science report: Climate change projections *Rep*, Met Office Hadley Centre, Exeter.
Naik, P. K., and D. A. Jay (2011), Distinguishing human and climate influences on the Columbia River: Changes in mean flow and sediment transport, *J. Hydrol.*, *404*(3–4), 259–277, doi:10.1016/j.jhydrol.2011.04.035.
Nearing, M. A. (2001), Potential changes in rainfall erosivity in the U.S. with climate change during the 21st century, *J. Soil Water Conserv.*, *56*(3), 229–232.
Nearing, M. A., G. R. Foster, L. J. Lane, and S. C. Finkner (1989), A process-based soil-erosion model for USDA-water erosion prediction project technology, *Trans. Asae*, *32*(5), 1587–1593.
Nearing, M. A., J. R. Simanton, L. D. Norton, S. J. Bulygin, and J. Stone (1999), Soil erosion by surface water flow on a stony, semiarid hillslope, *Earth Surf. Processes Landforms*, *24*(8), 677–686, doi:10.1002/(Sici)1096-9837(199908)24:8<677::Aid-Esp981>3.0.Co;2-1.
Nearing, M. A., et al. (2005), Modeling response of soil erosion and runoff to changes in precipitation and cover, *Catena*, *61*(2-3), 131–154, doi:10.1016/j.catena.2005.03.007.
Nearing, M. A., M. H. Nichols, J. J. Stone, K. G. Renard, and J. R. Simanton (2008), Sediment yields from unit-source semiarid watersheds at Walnut, *Water Resour. Res.*, *44*, W06426, doi:10.1029/2008WR006907.

Neitsch, S. L., J. G. Arnold, J. R. Kiniry, J. R. Williams, and K. W. King (2002), Soil and water assessment tool theoretical documentation, *TWRI Rep. TR-191,* Tex. Water Resour. Inst., College Station.
Nichols, M. H., J. J. Stone, and M. A. Nearing (2008), Sediment database, Walnut Gulch Experimental Watershed, Arizona, United States, *Water Resour. Res.*, *44*, W05S06, doi:10.1029/2006WR005682.
Nicks, A. D., and G. A. Gander (1994), CLIGEN: A weather generator for climate inputs to water resource and other models, paper presented at 5th International Conference on Computers in Agriculture, Orlando, Fla.
Nunes, J. P., and M. A. Nearing (2010), Modelling impacts of climatic change: Case studies using the new generation of erosion models, in *Handbook of Erosion Modelling*, pp. 289–312, John Wiley, Chichester, U. K.
Nunes, J. P., G. N. Vieira, J. Seixas, P. Gonclaves, and N. Carvalhais (2005), Evaluating the MEFIDIS model for runoff and soil erosion prediction during rainfall events, *Catena*, *61*(2-3), 210–228, doi:10.1016/j.catena.2005.03.005.
Nunes, J. P., J. Seixas, and N. R. Pacheco (2008), Vulnerability of water resources, vegetation productivity and soil erosion to climate change in Mediterranean watersheds, *Hydrol. Processes*, *22*(16), 3115–3134, doi:10.1002/Hyp.6897.
Nunes, J. P., J. Seixas, and J. J. Keizer (2013), Modeling the response of within-storm runoff and erosion dynamics to climate change in two Mediterranean watersheds: A multi-model, multi-scale approach to scenario design and analysis, *Catena*, *102*, 27–39, doi:10.1016/j.catena.2011.04.001.
O'Neal, M. R., M. A. Nearing, R. C. Vining, J. Southworth, and R. A. Pfeifer (2005), Climate change impacts on soil erosion in Midwest United States with changes in crop management, *Catena*, *61*(2–3), 165–184, doi:10.1016/j.catena.2005.03.003.
Osborn, H. B. (1983), Timing and duration of high rainfall rates in the southwestern United States, *Water Resour. Res.*, *19*(4), 1036–1042, doi:10.1029/WR019i004p01036.
Osterkamp, W. R., C. R. Hupp, and M. R. Schening (1995), Little River revisited — Thirty-five years after Hack and Goodlett, *Geomorphology*, *13*(1–4), 1–20, doi:10.1016/0169-555x(95)00063-b.
Parsons, A. J., J. Wainwright, R. E. Brazier, and D. M. Powell (2006), Is sediment delivery a fallacy?, *Earth Surf. Processes Landforms*, *31*(10), 1325–1328, doi:10.1002/esp.1395.
Paschalis, A., P. Molnar, S. Fatichi, and P. Burlando (2014), On temporal stochastic modeling of precipitation, nesting models across scales, *Adv. Water Resour.*, *63*(0), 152–166, doi:10.1016/j.advwatres.2013.11.006.
Peixoto, J. P., and A. H. Oort (1992), *The Physics of Climate*, Springer, New York.
Penman, H. L. (1948), Natural evaporation from open water, bare soil and grass, *Proc. R. Soc. A: Math. Phys. Eng. Sci.*, *193*(1032), 120–145, doi:10.1098/rspa.1948.0037.
Phan, D. B., C. C. Wu, and S. C. Hsieh (2011), Impact of climate change on stream discharge and sediment yield in Northern Viet Nam, *Water Resour.*, *38*(6), 827–836, doi:10.1134/s0097807811060133.
Polyakov, V. O., M. A. Nearing, M. H. Nichols, R. L. Scott, J. J. Stone, and M. P. McClaran (2010), Long-term runoff and sediment yields from small semiarid watersheds in southern Arizona, *Water Resour. Res.*, *46*, W09512, doi:10.1029/2009WR009001.
Pruski, F. F., and M. A. Nearing (2002a), Runoff and soil-loss responses to changes in precipitation: A computer simulation study, *J. Soil Water Conserv.*, *57*(1), 7–16.
Pruski, F. F., and M. A. Nearing (2002b), Climate-induced changes in erosion during the 21st century for eight U.S. locations, *Water Resour. Res.*, *38*(12), 1298, doi: 10.1029/2001WR000493.
Räisänen, J. (2007), How reliable are climate models?, *Tellus A*, *59*(1), 2–29, doi:10.1111/j.1600-0870.2006.00211.x.
Renard, K. G., L. J. Lane, J. R. Simanton, W. E. Emmerich, J. J. Stone, M. A. Weltz, D. C. Goodrich, and D. S. Yakowitz (1993), Agricultural impacts in an arid environment: Walnut Gulch studies, *Hydrol. Sci. Technol.*, *9*, 145–190.
Riebe, C. S., J. W. Kirchner, D. E. Granger, and R. C. Finkel (2001), Minimal climatic control on erosion rates in the Sierra Nevada, California, *Geology*, *29*(5), 447–450, doi:10.1130/0091-7613(2001)029<0447:Mccoer>2.0.Co;2.
Rinehart, A. J., E. R. Vivoni, and P. D. Brooks (2008), Effects of vegetation, albedo, and solar radiation sheltering on the solution of snow in the Valles Caldera, New Mexico, *Ecohydrology*, *1*, 253–270.
Ritchie, J. C., M. A. Nearing, M. H. Nichols, and C. A. Ritchie (2005), Patterns of soil erosion and redeposition on Lucky Hills Watershed, Walnut Gulch experimental watershed, Arizona, *Catena*, *61*(2–3), 122–130, doi:10.1016/j.catena.2005.03.012.
Roering, J. J., J. W. Kirchner, and W. E. Dietrich (2001), Hillslope evolution by nonlinear, slope-dependent transport: Steady state morphology and equilibrium adjustment timescales, *J. Geophys. Res.*, *106*(B8), 16,499–16,513, doi:10.1029/2001JB000323.
Römkens, M. J. M., K. Helming, and S. N. Prasad (2002), Soil erosion under different rainfall intensities, surface roughness, and soil water regimes, *Catena*, *46*(2–3), 103–123, doi:10.1016/s0341-8162(01)00161-8.
Routschek, A., J. Schmidt, W. Enke, and T. Deutschlaender (2014), Future soil erosion risk - Results of GIS-based model simulations for a catchment in Saxony/Germany, *Geomorphology*, *206*, 299–306, doi:10.1016/j.geomorph.2013.09.033.
Rutter, A. J., P. C. Robins, A. J. Morton, and K. A. Kershaw (1972), Predictive model of rainfall interception in forests. 1. Derivation of model from observations in a plantation of corsican pine, *Agric. Meteorol.*, *9*(5–6), 367–384.
Rutter, A. J., A. J. Morton, and P. C. Robins (1975), A predictive model of rainfall interception in forests. II Generalization of the model and comparison with observations in some coniferous and hardwood stands, *J. Appl. Ecol.*, *12*(1), 367–380.
Salles, C., J. Poesen, and G. Govers (2000), Statistical and physical analysis of soil detachment by raindrop impact: Rain erosivity indices and threshold energy, *Water Resour. Res.*, *36*(9), 2721–2729, doi:10.1029/2000WR900024.
Seager, R. (2007), The turn of the century North American drought: Global context, dynamics, and past analogs, *J. Clim.*, *20*(22), 5527–5552, doi:10.1175/2007jcli1529.1.
Seager, R., et al. (2007), Model projections of an imminent transition to a more arid climate in southwestern North America, *Science*, *316*(5828), 1181–1184, doi:10.1126/science.1139601.
Sheppard, P. R., A. C. Comrie, G. D. Packin, K. Angersbach, and M. K. Hughes (2002), The climate of the US Southwest, *Clim. Res.*, *21*(3), 219–238, doi:10.3354/Cr021219.
Shrestha, B., M. S. Babel, S. Maskey, A. van Griensven, S. Uhlenbrook, A. Green, and I. Akkharath (2013), Impact of climate change on sediment yield in the Mekong River basin: A case study of the Nam Ou basin, Lao PDR, *Hydrol. Earth Syst. Sci.*, *17*(1), 1–20, doi:10.5194/hess-17-1-2013.
Simonoff, J. S. (1996), *Smoothing Methods in Statistics*, Springer, New York.
Simons, D. B., and F. Şentürk (1992), *Sediment Transport Technology: Water and Sediment Dynamics*, Water Resour. Publ., Littleton, Colo.
Skirvin, S., M. Kidwell, S. Biedenbender, J. P. Henley, D. King, C. H. Collins, S. Moran, and M. Weltz (2008), Vegetation data, Walnut Gulch Experimental Watershed, Arizona, United States, *Water Resour. Res.*, *44*, W05S08, doi:10.1029/2006WR005724.
Slingo, A. (1989), A GCM parameterization for the shortwave radiative properties of water clouds, *J. Atmos. Sci.*, *46*(10), 1419–1427, doi:10.1175/1520-0469(1989)046<1419:agpfts>2.0.co;2.

Stephens, G. L. (1978), Radiation profiles in extended water clouds. II: Parameterization schemes, *J. Atmos. Sci.*, *35*(11), 2123–2132, doi:10.1175/1520-0469(1978)035<2123:rpiewc>2.0.co;2.

Stone, J. J., M. H. Nichols, D. C. Goodrich, and J. Buono (2008), Long-term runoff database, Walnut Gulch Experimental Watershed, Arizona, United States, *Water Resour. Res.*, *44*, W05S05, doi:10.1029/2006WR005733.

Styczen, M., and K. Høgh-Schmidt (1988), A new description of splash erosion in relation to raindrop sizes and vegetation, in *Erosion Assessment and Modelling*, edited by R. P. C. Morgan and R. J. Rickson, *Commission of the European Communities Rep. EUR 10860 EN*, pp. 147–184, Brussels.

Tebaldi, C., L. O. Mearns, D. Nychka, and R. L. Smith (2004), Regional probabilities of precipitation change: A Bayesian analysis of multimodel simulations, *Geophys. Res. Lett.*, *31*, D18123, doi:10.1029/2004GL021276.

Tebaldi, C., R. L. Smith, D. Nychka, and L. O. Mearns (2005), Quantifying uncertainty in projections of regional climate change: A Bayesian approach to the analysis of multimodel ensembles, *J. Clim.*, *18*(10), 1524–1540, doi:10.1175/Jcli3363.1.

Temme, A. J. A. M., J. E. M. Baartman, and J. M. Schoorl (2009), Can uncertain landscape evolution models discriminate between landscape responses to stable and changing future climate? A millennial-scale test, *Global Planet. Change*, *69*(1–2), 48–58, doi:10.1016/j.gloplacha.2009.08.001.

Tucker, G. E., and R. L. Bras (2000), A stochastic approach to modeling the role of rainfall variability in drainage basin evolution, *Water Resour. Res.*, *36*(7), 1953–1964, doi:10.1029/2000WR900065.

Tucker, G. E., and R. Slingerland (1997), Drainage basin responses to climate change, *Water Resour. Res.*, *33*(8), 2031–2047, doi:10.1029/97WR00409.

Tucker, G. E., S. T. Lancaster, N. M. Gasparini, and R. L. Bras (2001a), The Channel-Hillslope Integrated Landscape Development Model (CHILD), in *Landscape Erosion and Evolution Modeling*, edited by R. Harmon and W. Doe III, pp. 349–388, Springer.

Tucker, G. E., S. T. Lancaster, N. M. Gasparini, R. L. Bras, and S. M. Rybarczyk (2001b), An object-oriented framework for distributed hydrologic and geomorphic modeling using triangulated irregular networks, *Comput. Geosci.*, *27*(8), 959–973, doi:10.1016/S0098-3004(00)00134-5.

van Balen, R. T., F. S. Busschers, and G. E. Tucker (2010), Modeling the response of the Rhine–Meuse fluvial system to Late Pleistocene climate change, *Geomorphology*, *114*(3), 440–452, doi:10.1016/j.geomorph.2009.08.007.

Van De Wiel, M. J., T. J. Coulthard, M. G. Macklin, and J. Lewin (2007), Embedding reach-scale fluvial dynamics within the CAESAR cellular automaton landscape evolution model, *Geomorphology*, *90*(3–4), 283–301, doi:10.1016/j.geomorph.2006.10.024.

Vivoni, E. R., V. Y. Ivanov, R. L. Bras, and D. Entekhabi (2004), Generation of triangulated irregular networks based on hydrological similarity, *J. Hydrol. Eng.*, *9*(4), 288–302, doi:10.1061/(Asce)1084-0699(2004)9:4(288).

von Werner, M. (1995), GIS-orientierte Methoden der digitalen Reliefanalyse zur Modellierung von Bodenerosion in kleinen Einzugsgebieten.

Walling, D. E. (1983), The sediment delivery problem, *J. Hydrol.*, *65*(1–3), 209–237, doi:10.1016/0022-1694(83)90217-2.

Walling, D. E., and A. H. A. Kleo (1979), Sediment yields of rivers in areas of low precipitation: A global view, in *The Hydrology of Areas of Low Precipitation: Proceedings of an International Symposium*, edited by I. A. O. H. Sciences, pp. 479–493, IAHS-AISH, Exeter, U. K., 15–19 July 1996. [Available at https://books.google.it/books?id=bZ-ufVQV5yAC&dq=Sediment+yields+of+rivers+in+areas+of+low+precipitation:+a+global+view&hl=it&source=gbs_navlinks_s.]

Wang, H., R. Fu, A. Kumar, and W. H. Li (2010), Intensification of summer rainfall variability in the southeastern United States during recent decades, *J. Hydrometeorol.*, *11*(4), 1007–1018, doi:10.1175/2010jhm1229.1.

Welsh, K. E., J. A. Dearing, R. C. Chiverrell, and T. J. Coulthard (2009), Testing a cellular modelling approach to simulating late-Holocene sediment and water transfer from catchment to lake in the French Alps since 1826, *Holocene*, *19*(5), 785–798, doi:10.1177/0959683609105303.

Weltz, M. A., J. C. Ritchie, and H. D. Fox (1994), Comparison of laser and field measurements of vegetation height and canopy cover, *Water Resour. Res.*, *30*(5), 1311–1319, doi:10.1029/93WR03067.

Wicks, J. M., and J. C. Bathurst (1996), SHESED: A physically based, distributed erosion and sediment yield component for the SHE hydrological modelling system, *J. Hydrol.*, *175*(1–4), 213–238, doi:10.1016/S0022-1694(96)80012-6.

Wilby, R. L., and C. W. Dawson (2007), SDSM 4.2 — A decision support tool for the assessment of regional climate change impacts, Lancaster University, Lancaster/Environment Agency of England and Wales.

Willgoose, G., R. L. Bras, and I. Rodriguez-Iturbe (1991), A coupled channel network growth and hillslope evolution model: 1 Theory, *Water Resour. Res.*, *27*(7), 1671–1684, doi:10.1029/91WR00935.

Yalin, M. S. (1972), *Mechanics of Sediment Transport*, Pergamon Press, Oxford, U. K.

Yang, C. T. (1996), *Sediment Transport: Theory and Practice*, McGraw-Hill Higher Education, New York.

Zhang, P. Z., P. Molnar, and W. R. Downs (2001), Increased sedimentation rates and grain sizes 2–4 Myr ago due to the influence of climate change on erosion rates, *Nature*, *410*(6831), 891–897.

Zhang, X. C. (2007), A comparison of explicit and implicit spatial downscaling of GCM output for soil erosion and crop production assessments, *Clim. Change*, *84*(3–4), 337–363, doi:10.1007/s10584-007-9256-1.